# Analysis of shortest paths and subscriber line lengths in telecommunication access networks

C. Gloaguen[1] F. Fleischer [2,3] H. Schmidt [1] V. Schmidt [3]

3rd November 2006

**Abstract**

We consider random geometric models for telecommunication access networks and analyse their serving zones which can be given, for example, by a class of so–called Cox–Voronoi tessellations (CVTs). Such CVTs are constructed with respect to locations of network components, the nucleii of their induced cells, which are scattered randomly along lines induced by a Poisson line process. In particular, we consider two levels of network components and investigate these hierarchical models with respect to mean shortest path length and mean subscriber line length, respectively. We explain point–process techniques which allow for these characteristics to be computed without simulating the locations of lower–level components. We sustain our results by numerical examples which were obtained through Monte Carlo simulations, where we used simulation algorithms for typical Cox–Voronoi cells derived in a previous paper. Also, briefly, we discuss tests of correctness of the implemented algorithms. Finally, we present a short outlook to possible extensions concerning multi–level models and iterated random tessellations.
*Keywords* : TELECOMMUNICATION NETWORK MODELLING, STOCHASTIC GEOMETRY, POINT PROCESS, PALM PROBABILITY, NEVEU'S EXCHANGE FORMULA, SPATIAL TESSELLATION, TYPICAL COX–VORONOI CELL, ACCESS NETWORK, SHORTEST PATH, SUBSCRIBER LINE

## 1 Introduction

Spatial stochastic models have been developed in recent years as alternatives to more traditional economical approaches for cost measurement and strategic planning of telecommunication networks. These models incorporate both stochastic as well as geometric features observable in telecommunication networks. While the random setting reflects the network's variability in time and space, consideration of geometric structures of network architectures offer a more realistic view to location-dependent network characteristics than conventional models.

Prominent examples of networks where stochastic-geometric models have been considered recently are mobile telecommunication systems, multi-cast networks and switching networks. These new models using tools and methods of stochastic geometry are based on modulated

[1]France Télécom R&D RESA/NET/NSO 92131 Issy les Moulineaux Cedex 9, France
[2]Institute of Applied Information Processing and Institute of Stochastics, Ulm University, 89069 Ulm, Germany
[3]Institute of Stochastics, Ulm University, 89069 Ulm, Germany

Poisson–Voronoi tessellations ([6], [7]), Poisson–Voronoi aggregated tessellations ([3], [23]), superpositions of Poisson-Voronoi tessellations ([2]), spanning trees ([4], [5]), and coverage processes ([1]).

Bearing in mind the fact that roughly 50% of the total capital investment in telecommunication networks is made in access networks, their modelling and subsequent analysis can be considered as the most important part of telecommunication network modelling.

The access network or local loop is the part of the network connecting a subscriber to its corresponding Wire Center Stations (WCS). The hierarchical physical link is made via network components: a Network Interface Device (ND), secondary and primary cabinets (CS and CP) and a Service Area Station (SAI) as shown in Figure 1(a). To each WCS we associate a serving zone such that the inscribed subnetwork that gathers all lines between the WCS and the subscribers displays a tree structure; Figure 1(b).

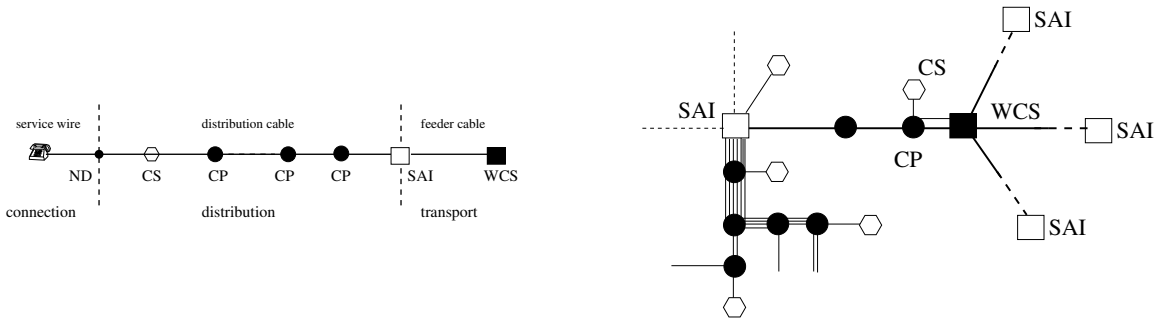


(a) *Hierarchical physical link between a subscriber and its Wire Center Station (WCS)*

(b) *Tree structure of a WCS subnetwok not displaying the links between ND ans CS*

Figure 1: Hierachical structure of access networks

The most important feature about the access network is that it is the place where the telecommunication network fits into the town and country infrastructure. In the following, we conveniently restrict ourselves to the description and analysis of urban access networks.

In recent years, access networks were studied in the context of the so-called Stochastic Subscriber Line Model (SSLM); see [10], [11], [12] and [14]. The SSLM is a random geometric model that offers tools to describe geometric features of access networks and that allows for stochastic econometrical analysis, like the analysis of connection costs.

The modelling framework of the SSLM can be subdivided into the network geometry model, the network component model, and the network topology model. The network geometry model represents the cable trench system, typically located along the urban infrastructure system, and in the SSLM modelled by random tessellations. Subsequently the network component model places technical network components along the cable trenches according to independent (Poisson) point processes on lines or in the plane. Finally the components are connected with respect to the network topology model.

Methods for an optimal choice of the geometry model with respect to given data can be found in [12]. In [11] an algorithm was introduced in order to simulate typical Cox-Voronoi cells based on linear Poisson processes on random lines. In the present paper, this algorithm, together with other techniques, is used to investigate two–level hierarchical models, i.e. models of two different components where the lower–level component is connected to its closest higher–level component, based on Poisson line tessellations. Efficient computation and

simulation techniques for network characteristics like mean shortest path length and mean subscriber line length are shown. These network characteristics can be key–ingredients to an efficient cost analysis. Notice that Poisson line tessellations are chosen as geometry model since earlier investigations showed that, for a lot of real data situations, they can represent a suitable model for the urban infrastructure.

The investigated stochastic network model that is based on a Poisson line tessellation and two hierarchically ordered stationary point processes that are located on the lines, is explained in Section 2. In Sections 3 and 4, a formal definition of the regarded network characteristics, mean shortest path length and mean subscriber line length, is given. We explain methods which allow for these characteristics to be computed without simulating the locations of lower–level components, thereby enhancing simulation speed enormously. In particular, instead of performing large–scale computations of shortest path lengths and subscriber line lengths, respectively, for each lower–level component individually, we first use an ergodicity argument by which these large–scale computations can be reduced to the computation of a single expectation value with respect to the so–called Palm probability measure induced by the point process of lower–level components. Then, we apply Neveu's exchange formula for stationary marked point processes. This allows us to pass to expectations with respect to the Palm probability measure induced by the point process of higher–level components, which are computationally easier to handle. Finally, we compute the latter expectations by partitioning the underlying line system and by applying inner Voronoi tessellations with respect to the edges of the cells formed by the Poisson line process. Section 5 shows numerical results of the computations performed for the two network characteristics mentioned above. Topics of run–time and of testing the implemented software are also discussed in this section. Section 6 gives a short outlook to possible extensions of the regarded models with respect to multi–level hierarchies and to more complicated geometry models. Mathematical background for the tools applied in this paper can be found in Appendix A whereas detailed proofs for the derived theorems are given in Appendix B.

All implementations that have been performed for the computation and the simulation of network characteristics and corresponding models are integrated in the GeoStoch library, which has been developed by the Institute of Applied Information Processing and the Institute of Stochastics of Ulm University. This JAVA–based library comprises software tools designed to analyze data with methods from stochastic geometry; see [17] and *http://www.geostoch.de*.

## 2 Stochastic modelling of telecommunication access networks

In order to model telecommunication access networks, different aspects have to be taken into account. First the geometry of the underlying infrastructure has to be modelled, which in most cases is represented by the (urban) street system. After this step, network equipment components have to be placed randomly on the streets or (spatially) within the cells formed by these streets. Finally, the connections between the equipment components have to be considered. This section specifies and explains the investigated stochastic models with respect to the choice of the geometry model as well as the choice of models for equipment placement and equipment connections.

In the following we regard two–level hierarchical models. They describe two different equipment types which are placed along the infrastructure system. More precisely, we start by considering a Poisson line process (cmp. Appendix A.5), which is intended to model the underlying road system. Given a realization of such an underlying line system we independently

generate either two (marked) point processes on each line, which can be seen as spatial point processes concentrated on the system of lines, or we generate one of the two point processes (the lower–level) within the cells formed by the lines of the underlying line system.

In such a setting, we have that for a linear placement of the lower–level point process the higher–level point process might represent for example the locations of the WCS, whereas the lower–level point process is intended to model the locations of the SAI. For a spatial placement of the lower–level point process the higher–level point process might represent the locations of the SAI, whereas the lower–level point process is a model for the locations of the subscribers.

## 2.1 Network geometry and higher-level components

As a model for the underlying infrastructure system, or in other words the network geometry, a Poisson line tessellation is chosen which is induced by a stationary and isotropic Poisson line process $X_\ell$ with intensity $\gamma$; see Figure 2(a) and Appendix A.7. The higher–level components are placed on the lines of this line system, in agreement with the rules defined by the SSLM. Furthermore, the locations of higher–order components are assumed to form a (non–marked) stationary point process $X_H = \{X_n\}_{n\geq 1}$ in $\mathbb{R}^2$ with intensity $\lambda_H$ (cmp. Appendix A.2).

Later on in Section 5, we will assume that $X_H$ is a doubly stochastic Poisson processs (also called Cox process) whose (random) intensity measure is concentrated on the lines of the underlying Poisson line pocess $X_\ell$; see Figure 2(b) and Appendix A.6. However, for the purposes of Sections 3 and 4, this assumption is unnecessarily strong. Thus, for the moment, we only assume that $X_H$ satisfies the following conditions. Given $X_\ell$, consider independent stationary and ergodic (linear) point processes on each line of $X_\ell$ and let $X_H$ be the superposition of these point processes. It is well known that their (linear) intensity $\lambda_1$, measured along the lines of $X_\ell$, is connected to the (full–dimensional) intensity $\lambda_H$ via

$$\lambda_H = \lambda_1 \gamma \,. \tag{2.1}$$

Furthermore, suppose that each location $X_n$ of a higher–level component has an influence zone $\Xi(X_n)$ and that the sequence $\{\Xi(X_n)\}_{n\geq 1}$ forms a Voronoi tessellation induced by $X_H$. If the process of higher–level components is given by a Cox process as described above we call the Voronoi tessellation induced by $X_H$ a *Cox–Voronoi tessellation* (CVT); see Figure 2(c) and Appendix A.7.

**Theorem 2.1** *Let $\Xi^*$ denote the typical cell of the Voronoi tessellation $\{\Xi(X_n)\}_{n\geq 1}$ induced by the stationary point process $X_H = \{X_n\}_{n\geq 1}$ of higher–level components. Then,*

$$\lambda_1 = \frac{1}{\mathbb{E}_{X_H} \nu_1(L(\Xi^*))} \,, \tag{2.2}$$

*where $\mathbb{E}_{X_H}$ denotes expectation with respect to the Palm probability measure $\mathbb{P}^*_{X_H}$ of $X_H$ (cmp. (A.10)) and where $L(\Xi^*)$ denotes the (Palm) line system within the typical cell $\Xi^*$.*

**Proof** Using (2.1) and the fact that the mean area of the typical cell of $X_H$ is the reciprocal of $\lambda_H$ (cmp. (A.16)), we get immediately that

$$\frac{1}{\lambda_1 \gamma} = \mathbb{E}_{X_H} \nu_2(\Xi^*) \,.$$

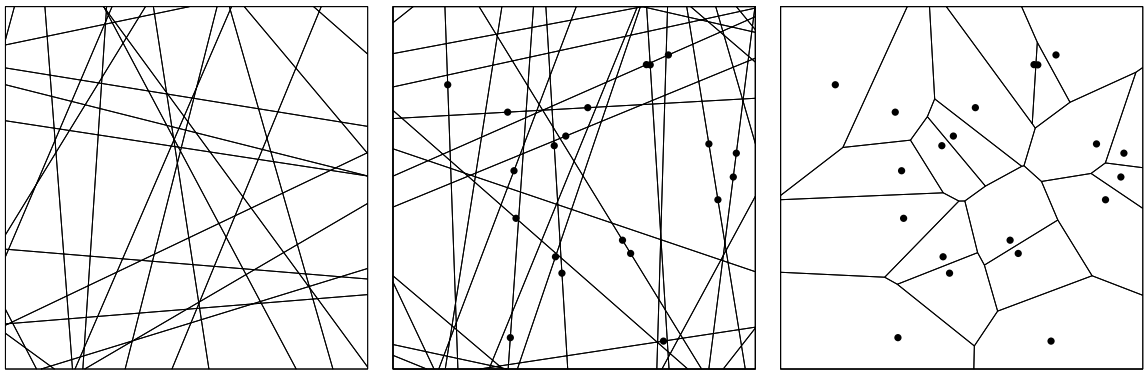

(a) *Poisson line process* (b) *Cox process* (c) *CVT*

Figure 2: Poisson line process and Cox–Voronoi tessellation (CVT)

Furthermore, we have $\mathbb{E}_{X_H}(\nu_1(L(\Xi^*))) = \gamma \mathbb{E}_{X_H}\nu_2(\Xi^*)$. This proves (2.2). □

Notice that, apart from Poisson line tessellations, the SSLM also allows for other choices of geometry models, depending on the given real data; see [12].

## 2.2 Lower–level components and shortest paths

With respect to the placement of lower–level components two different scenarios are regarded. In a first scenario, given $X_\ell$, the lower–level components are placed according to independent Poisson point processes with (linear) intensity $\lambda_2$ on the lines of the Poisson line process $X_\ell$; see Fig. 3(a). Then, the union $\{\widetilde{X}_n\}_{n\geq 1}$ of all locations $\widetilde{X}_n$ of lower–level components forms a stationary (doubly stochastic Poisson) point process in $\mathbb{R}^2$ whose (planar) intensity is denoted by $\lambda_L$. Notice that similar to the situation considered in (2.1), $\lambda_2$ can be connected to $\lambda_L$ via $\lambda_L = \lambda_2\gamma$.

To exclude trivial cases, we always assume in this paper that $0 < \lambda_H, \lambda_L < \infty$.

Let $N(\widetilde{X}_n)$ denote the location of the nearest (in the Euclidean sense) higher–level component of $\widetilde{X}_n$ and let $P(\widetilde{X}_n, N(\widetilde{X}_n))$ be the shortest path from $\widetilde{X}_n$ to $N(\widetilde{X}_n)$ along the edges of the graph induced by the Poisson line process $X_\ell$; see Figure 4 and Appendix A.8. By $c(P(\widetilde{X}_n, N(\widetilde{X}_n)))$ we denote the length of the path $P(\widetilde{X}_n, N(\widetilde{X}_n))$.

An important network characteristic of special interest is the mean shortest path length, i.e., the average distance with respect to the underlying graph structure from the lower–level components to their nearest (in the Euclidean sense) higher–level components. In order to analyze this characteristic, each location $\widetilde{X}_n$ of the lower–level components is associated with the mark $c(P(\widetilde{X}_n, N(\widetilde{X}_n))) > 0$. This leads to the stationary marked point process (cmp. Appendix A.3)

$$X_L = \{[\widetilde{X}_n, c(P(\widetilde{X}_n, N(\widetilde{X}_n)))]\}_{n\geq 1}\,, \tag{2.3}$$

whose mark space is the non–negative $x$–axis $[0, \infty)$.

In a second scenario, the lower–level components are not placed on the edges, but into the cells formed by the Poisson line process $X_\ell$, according to an independent (stationary) Poisson point process $\{X'_n\}_{n\geq 1}$ in $\mathbb{R}^2$ with (planar) intensity $\lambda_L$. Afterwards, for each $n$, the location $X'_n$ of the $n$th lower–level component is connected with the location $N(X'_n)$ of its nearest (in the Euclidean sense) higher–level component. This is done in the following way.

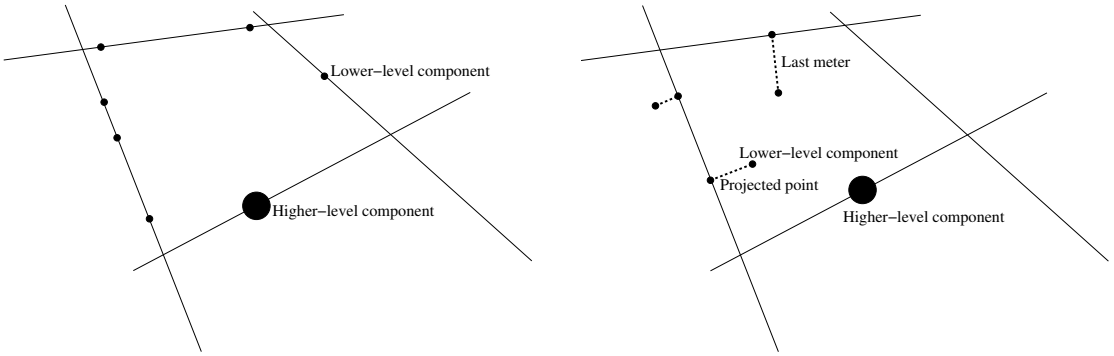


(a) *Linear placement on lines* (b) *Spatial placement and projection to nearest line*

Figure 3: Two scenarios for the placement of lower-level components

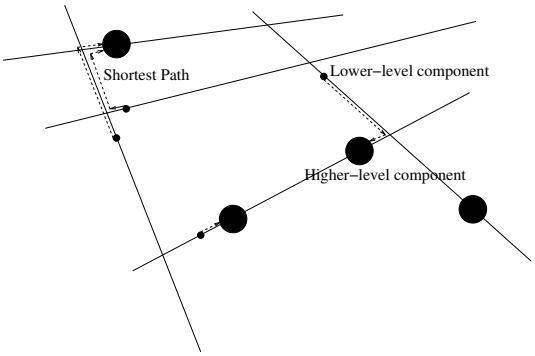


Figure 4: Some sample shortest paths from a lower–level to a higher–level component

Let $\Xi_n = \Xi(N(X'_n))$ be the Voronoi cell of $N(X'_n)$ and let $L(\Xi_n)$ denote the restriction of the Poisson line process $X_\ell$ to $\Xi_n$. Then, the location $X'_n$ is first connected to its nearest point of the line system $L(\Xi_n)$; see Figure 3(b). This "projection point" is denoted by $X''_n$. We are interested in the mean subscriber line length, representing the average shortest distance of the projected points $X''_n$ on the lines to the locations $N(X'_n)$ of their higher–order components, with respect to the underlying graph structure induced the Poisson line process $X_\ell$. Again, these distances can be expressed via the marks $c(P(X'_n, N(X'_n)))$, attached to the locations $X'_n$ of lower–level components. However, in this second placement scenario, one can split up the marks according to

$$c(P(X'_n, N(X'_n))) = c'(X'_n, X''_n) + c(P(X''_n, N(X'_n)))\,, \tag{2.4}$$

where $c'(X'_n, X''_n)$ is the cost value of the "edge" with respective endpoints $X'_n$ and $X''_n$. Note that in Section 5, we assume $c'(X'_n, X''_n) = 0$ in order to enhance the clarity of presentation.

# 3 Mean shortest path length

In this section we investigate the mean shortest path length for the first location scenario of lower–level components described in Section 2.2.

## 3.1 Simulation methods

At first glance, a natural approach in order to practically analyze the mean shortest path length seems to be the following procedure. First, simulate the network in a (supposedly large) sampling window $W \subset \mathbb{R}^2$, then compute the shortest path length $c(P(\widetilde{X}_n, N(\widetilde{X}_n)))$ for each location $\widetilde{X}_n$ of lower–level components generated in the sampling window, and, finally compute the average $c_{LH}(W)$ of these shortest path lengths, where

$$c_{LH}(W) = \frac{1}{\#\{n : \widetilde{X}_n \in W\}} \sum_{n\geq 1} \mathbb{1}_W(\widetilde{X}_n) c(P(\widetilde{X}_n, N(\widetilde{X}_n)))\,. \tag{3.1}$$

However, it becomes very rapidly clear that this method has some distinct disadvantages. If the sampling window $W$ is too small, the problem of edge–effects is significant. If, on the other hand, $W$ is large, the computational problem arises that a lot of memory and runtime is needed for single simulation runs.

Therefore, we propose an alternative approach by using the Palm probability measure $\mathbb{P}^*_{X_L}$ of the stationary marked point process $X_L = \{[\widetilde{X}_n, c(P(\widetilde{X}_n, N(\widetilde{X}_n)))]\}_{n\geq 1}$; see (2.3) and (A.10). This alternative approach is based on the following asymptotic property of the random variable $c_{LH}(W)$ defined in (3.1). Let $\{W_i\}_{i\geq 1}$ be a so–called averaging sequence of unboundedly increasing sampling windows; see [8]. Then, by the ergodicity of the stationary marked point process $X_L$, we have that

$$\lim_{i\to\infty} c_{LH}(W_i) = c^*_{LH} \tag{3.2}$$

holds with probability 1, where

$$c^*_{LH} = \frac{1}{\lambda_L \nu_2(B)}\, \mathbb{E} \sum_{n\geq 1} \mathbb{1}_B(\widetilde{X}_n) c(P(\widetilde{X}_n, N(\widetilde{X}_n))) = \mathbb{E}_{X_L} c(P(o, N(o)))\,. \tag{3.3}$$

Recall that the symbol $B$ in (3.3) means an arbitrary (bounded) Borel set $B \in \mathcal{B}(\mathbb{R}^2)$ with $0 < \nu_2(B) < \infty$ and $\mathbb{E}_{X_L}$ denotes expectation with respect to the Palm probability measure $\mathbb{P}^*_{X_L}$ introduced in (A.10).

Thus, motivated by the limit theorem given in (3.2), we will compute the expectation $c^*_{LH} = \mathbb{E}_{X_L} c(P(o, N(o)))$, which will be much easier than computing the average $c_{LH}(W)$ given in (3.1). Moreover, by Neveu's exchange formula stated in Theorem A.1, we can express $c^*_{LH}$ in an even more favorable way; see Section 3.2.

## 3.2 Application of Neveu's formula

The following result admits a practically more feasible representation of the expectation $c^*_{LH} = \mathbb{E}_{X_L} c(P(o, N(o)))$ appearing in (3.2) and, in the consequence, a more efficient way to approximately compute the mean shortest path length $c_{LH}(W)$ considered in (3.1).

**Theorem 3.1** *Consider the point process $X_H = \{X_n\}_{n\geq 1}$ of locations of higher–level components and the (marked) point process $X_L = \{[\widetilde{X}_n, c(P(\widetilde{X}_n, N(\widetilde{X}_n)))]\}_{n\geq 1}$. Then,*

$$\mathbb{E}_{X_L}\, c(P(o, N(o))) = \frac{1}{\mathbb{E}_{X_H} \nu_1(L(\Xi^*))}\, \mathbb{E}_{X_H} \int_{L(\Xi^*)} c(P(u, o))\, du\,, \tag{3.4}$$

*where $\Xi^*$ denotes the typical cell of the Voronoi tessellation induced by $X_H$ and $L(\Xi^*)$ is the (Palm) line system within $\Xi^*$.*

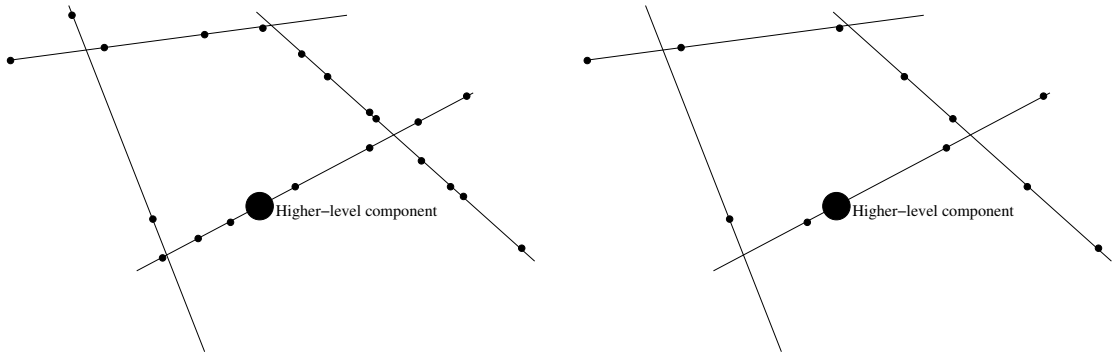


(a) *High intensity* (b) *Low intensity*

Figure 5: The intensity of lower-level components

A proof of Theorem 3.1 is given in Appendix B. Notice that Theorem 3.1 is a consequence of Neveu's exchange formula for Palm distributions (cmp. A.11 and [19]). Neveu's exchange formula is a very widely used tool in different kinds of applications in order to express the relationship of expectations for functionals of two stationary point processes with respect to their Palm distributions ([2], [5], [18], [21]).

By (3.4), we can further simplify the computation of the mean shortest path length $c_{LH}(W)$ considered in (3.1). Namely, instead of computing the expectation $c^*_{LH} = \mathbb{E}_{X_L} c(P(o, N(o)))$ appearing in (3.2), we will estimate the quotient of expectations on the right–hand side of (3.4). For doing so, we just have to simulate the typical serving zone $\Xi^*$ of higher–level components, together with their corresponding (typical) line system, where $L(\Xi^*)$ denotes this line system restricted to $\Xi^*$.

We also remark that the expression for $\mathbb{E}_{X_L} c(P(o, N(o)))$ given in (3.4) can be alternatively written in the form

$$\mathbb{E}_{X_L}\, c(P(o, N(o))) = \lambda_1\, \mathbb{E}_{X_H} \int_{L(\Xi^*)} c(P(u, o))\, du\,, \tag{3.5}$$

which immediately follows from Theorems 2.1 and 3.1. This shows in particular that the expectation $\mathbb{E}_{X_L} c(P(o, N(o)))$ does actually not depend on $\lambda_2$; see also Figure 5.

### 3.3 Computational algorithm

In order to get an estimator $\widehat{c}_{LH}$ for $c^*_{LH}$, we use the expression (3.4) derived in Theorem 3.1. The idea is to simulate the typical Voronoi cell $\Xi^*$, and the (typical) line system $L(\Xi^*)$, a certain number of times, $k$ say. Furthermore, we partition the line system $L(\Xi^*_i)$ in $\Xi^*_i$ for $i = 1, \ldots, k$ into its line segments $E_i = \{S_i^{(1)}, S_i^{(2)} .., S_i^{(M_i)}\}$, where $M_i$ is the total number of line segments in $\Xi^*_i$ for $1 \le i \le k$. Notice that the line which contains the origin is subdivided into two segments; see Figure 6(a).

Hence, taking classical sample means, we get that $\lim_{k\to\infty} \widehat{c}_{LH}(k) = c^*_{LH}$ with probability 1, where

$$\widehat{c}_{LH}(k) = \frac{1}{\frac{1}{k}\sum\limits_{i=1}^{k} \nu_1(L(\Xi^*_i))}\, \frac{1}{k} \sum_{i=1}^{k} \sum_{j=1}^{M_i} \int_{S_i^{(j)}} c(P(u, o))\, du\,,$$

i.e.,

$$\widehat{c}_{LH}(k) = \frac{1}{\sum_{i=1}^{k} \nu_1(L(\Xi_i^*))} \sum_{i=1}^{k} \sum_{j=1}^{M_i} \int_{S_i^{(j)}} c(P(u,o))\, du\,. \tag{3.6}$$

Notice that the intensity $\lambda_1$ is known in some cases. Then, alternatively, we can use the relationship (3.5) in order to get still another estimator $\check{c}_{LH}(k)$ for $c_{LH}^*$, where

$$\check{c}_{LH}(k) = \lambda_1 \frac{1}{k} \sum_{i=1}^{k} \sum_{j=1}^{M_i} \int_{S_i^{(j)}} c(P(u,o))\, du\,. \tag{3.7}$$

In both cases, it remains to know how the integrals on the right–hand sides of (3.6) and (3.7), respectively, can be computed. This is shown in the following theorem, where some additional assumptions will be made on the cost function $c : E \to [0,\infty)$ introduced in Section A.8.

**Theorem 3.2** *Suppose that the values $c(e)$ of the cost function $c : E \to [0,\infty)$ only depend on the lengths of the edges $e \in E$ and that $c(e)$ is monotonously increasing with respect to the length of $e$, where $c(e) = 0$ if $\nu_1(e) = 0$. Let $S = S(A,B)$ be a line segment with respective endpoints $A$ and $B$, and let $\delta_S = c(P(B,o)) - c(P(A,o))$. Then,*

$$c(P(A,B)) \geq |\delta_S|\,. \tag{3.8}$$

*Moreover, there exists a point $D \in S$ such that*

$$c(P(A,o)) + c(P(D,A)) = c(P(B,o)) + c(P(D,B)) \tag{3.9}$$

*and*

$$\begin{aligned} \int_S c(P(u,o))\, du &= c(P(A,o))\nu_1(D-A) + \int_D^A c(P(A,u))\, du \\ &\quad + c(P(B,o))\nu_1(D-B) + \int_D^B c(P(B,u))\, du\,. \end{aligned} \tag{3.10}$$

**Corollary 3.3** *If $c(S)$ is the length of the segment $S = S(A,B)$, i.e. $c(S) = \nu_1(S)$, then*

$$\int_S c(P(u,o))\, du = f(\nu_1(S); c(P(A(S),o)), c(P(B(S),o)))\,, \tag{3.11}$$

*where*

$$f(x;\theta_1,\theta_2) = \frac{1}{4}x^2 + \frac{1}{2}(\theta_1+\theta_2)x - \frac{1}{4}(\theta_2-\theta_1)^2\,. \tag{3.12}$$

Proofs of Theorem 3.2 and of Corollary 3.3 are given in Appendix B.

If $c(e) = \nu_1(e)$ for any $e \in E_i$ for $i = 1,\ldots,k$ and $k \geq 1$ then by Corollary 3.3, we immediately get the following final expressions for the estimators $\widehat{c}_{LH}(k)$ and $\check{c}_{LH}(k)$.

**Corollary 3.4** *For each $k \geq 1$ let $E_i = \{S_i^{(j)}\}_{j=1}^{M_i}$ be the partion of the line system $L(\Xi_i^*)$ restricted to the $i$th typical cell $\Xi_i^*$ for $i = 1,\ldots,k$ and let $A_i^{(j)}$ and $B_i^{(j)}$, respectively, denote the endpoints of the segment $S_i^{(j)}$. Then,*

$$\widehat{c}_{LH}(k) = \frac{1}{\sum_{i=1}^{k} \nu_1(L(\Xi_i^*))} \sum_{i=1}^{k} \sum_{j=1}^{M_i} f(\nu_1(S_i^{(j)}); c(P(A_i^{(j)}),o), c(P(B_i^{(j)},o))) \tag{3.13}$$

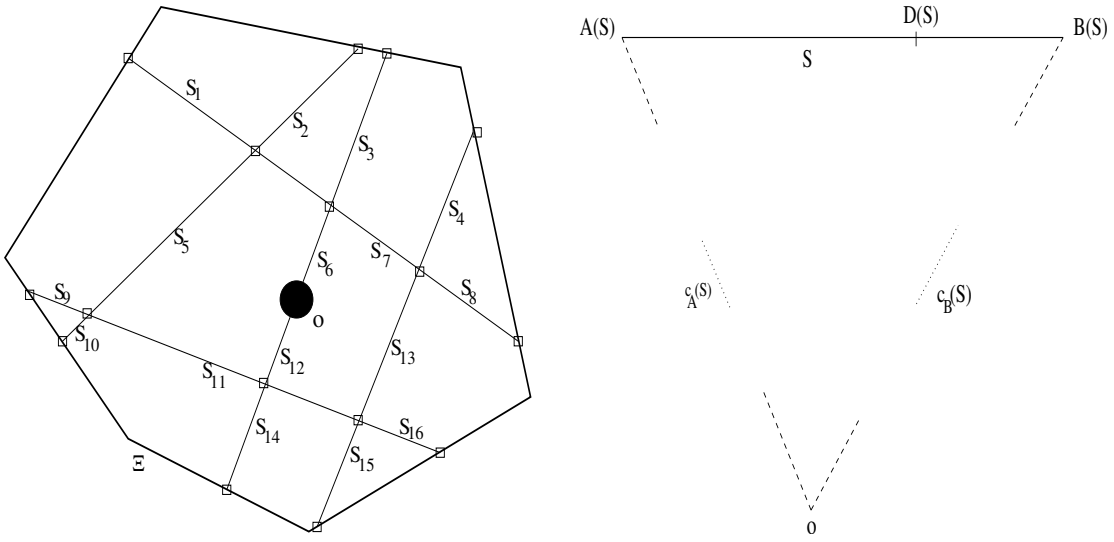


(a) *Partitioning of* $L(\Xi_i^*)$ *into segments* (b) *Mean shortest path length for single segment*

Figure 6: Partitioning and weighted mean shortest path length

*and*

$$\check{c}_{LH}(k) = \frac{\lambda_1}{k} \sum_{i=1}^{k} \sum_{j=1}^{M_i} f(\nu_1(S_i^{(j)}); c(P(A_i^{(j)}), o), c(P(B_i^{(j)}, o))) \,, \tag{3.14}$$

*where the function* $f$ *is given in* (3.12).

By the representation formulae (3.13) and (3.14), it suffices to compute the path lengths $c(P(A_i^{(j)}), o)$ and $c(P(B_i^{(j)}), o)$ for $j = 1, \ldots, M_i$ and $i = 1, \ldots, k$ in order to determine the estimators $\widehat{c}_{LH}(k)$ and $\check{c}_{LH}(k)$. This can be done, for example, by applying Dijkstra's algorithm; see Section 5 below.

# 4 Mean subscriber line length

In this section we consider the case, where the lower–level components are not placed on the edges, but into the cells formed by the Poisson line process $X_\ell$, according to an independent (stationary) Poisson point process $\{X_n'\}_{n\geq 1}$ in $\mathbb{R}^2$ with (planar) intensity $\lambda_L$; see Section 2.2.

Recall that, for each $n$, the location $X_n'$ of the $n$th lower–level component is connected with the location $N(X_n')$ of its nearest (in the Euclidean sense) higher–level component. For this purpose, $X_n'$ is first connected to its nearest point $X_n''$ of the line system $L(\Xi_n)$, where $\Xi_n = \Xi(N(X_n'))$ is the Voronoi cell of $N(X_n')$ and $L(\Xi_n)$ denotes the restriction of the Poisson line process $X_\ell$ to $\Xi_n$.

An interesting characteristic is the so–called mean subscriber line length

$$d_{LH}(W) = \frac{1}{\#\{n : X_n' \in W\}} \sum_{n\geq 1} \mathbb{1}_W(X_n')\, c(P(X_n', N(X_n'))) \tag{4.1}$$

for some sampling window $W \subset \mathbb{R}^2$, where the cost value $c(P(X_n', N(X_n')))$ of the shortest path from $X_n'$ to $N(X_n'))$ is given in (2.4).

## 4.1 Simulation and usage of Neveu's formula

In order to practically analyze the mean subscriber line length $d_{LH}(W)$, we propose an approach which is analogous to that considered in Section 3, i.e. an approach based on the Palm probability measure $\mathbb{P}^*_{X'_L}$ of the stationary marked point process $X'_L = \{[X'_n, c(X'_n)]\}_{n\geq 1}$, where $c(X'_n) = c(P(X'_n, N(X'_n)))$. Then, by the ergodicity of $X'_L$, we have that

$$\lim_{i\to\infty} d_{LH}(W_i) = d^*_{LH} \tag{4.2}$$

holds with probability 1, where $\{W_i\}_{i\geq 1}$ is an averaging sequence of unboundedly increasing sampling windows and

$$d^*_{LH} = \frac{1}{\lambda_L \nu_2(B)}\, \mathbb{E} \sum_{n\geq 1} \mathbb{1}_B(X'_n)\, c(P(X'_n, N(X'_n))) = \mathbb{E}_{X'_L} c(P(o, N(o))) \tag{4.3}$$

for some (bounded) Borel set $B \in \mathcal{B}(\mathbb{R}^2)$ with $0 < \nu_2(B) < \infty$.

Furthermore, applying Neveu's exchange formula (A.11), we get the following expression for the expectation $\mathbb{E}_{X'_L} c(P(o, N(o)))$ appearing in (4.3).

**Theorem 4.1** *Consider the point process $X_H = \{X_n\}_{n\geq 1}$ of higher–level components and the (marked) point process $X'_L = \{[X'_n, c(P(X'_n, N(X'_n)))]\}_{n\geq 1}$. Then,*

$$\mathbb{E}_{X'_L}\, c(P(o, N(o))) = \frac{1}{\mathbb{E}_{X_H} \nu_2(\Xi^*)}\, \mathbb{E}_{X_H} \int_{\Xi^*} c(P(u, o))\, du\,, \tag{4.4}$$

*where $\Xi^*$ denotes the typical cell of the Voronoi tessellation induced by $X_H$.*

A proof of Theorem 4.1 can be found in Appendix B.

## 4.2 Computation via inner Voronoi cells

Using (4.3) and (4.4), we get an estimator $\widehat{d}_{LH}$ for the limit $d^*_{LH}$ considered in (4.2). Again we start by simulating the typical line system and the typical Voronoi cell $\Xi^*$ with respect to the higher–level components $k$ times, getting $k$ independent and identically distributed copies $\Xi^*_1, \ldots, \Xi^*_k$ of $\Xi^*$, where $k > 0$ is an arbitrary fixed integer. In Figure 7 two samples for the typical Voronoi cell are displayed. Apart from the nucleus (thick dot), the cell itself (thick lines), and the underlying line system (medium lines), the so–called inner Voronoi tessellation with respect to the underlying line system is displayed (thin lines). The cells of the inner Voronoi tessellation are formed with respect to the edges of the cells of the underlying line system.

Notice however that there are no inner Voronoi cells with respect to the boundary of the typical Voronoi cell $\Xi^*$, since obviously, a lower–level point should be projected solely to a segment of the underlying line system $L(\Xi^*)$ restricted to $\Xi^*$. For example, in the realization of the typical Voronoi cell $\Xi^*$ shown at the right–hand side of Figure 7, all points of the small triangle in the left–upper corner are projected onto an „isolated" segment of the line system $L(\Xi^*)$. This means that the shortest path from these points to the corresponding higher–level component, located at the origin, is *not* completely contained in the typical Voronoi cell $\Xi^*$.

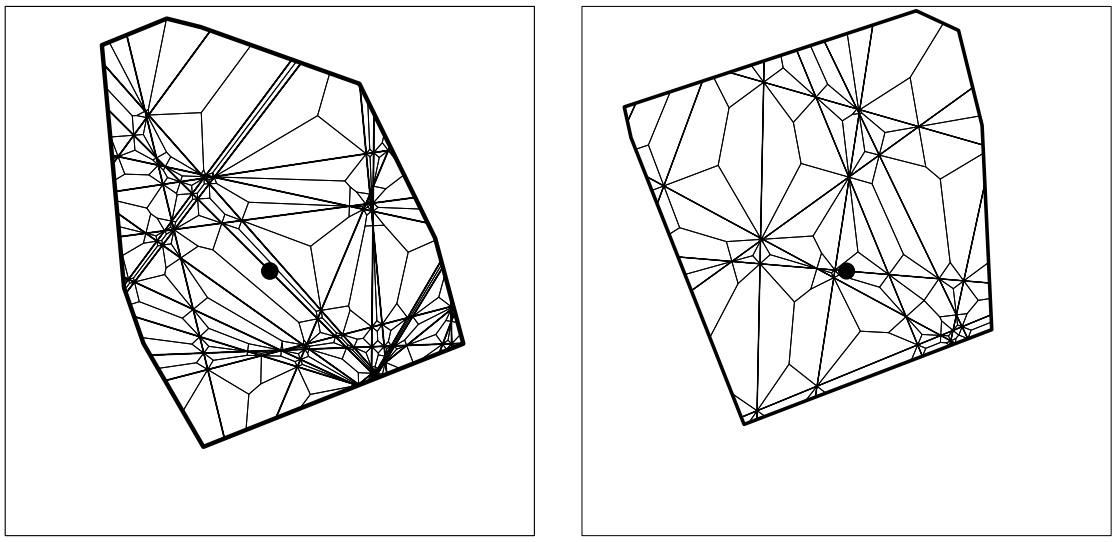

Figure 7: Samples for the typical Voronoi cell with underlying line structure and inner Voronoi tessellation

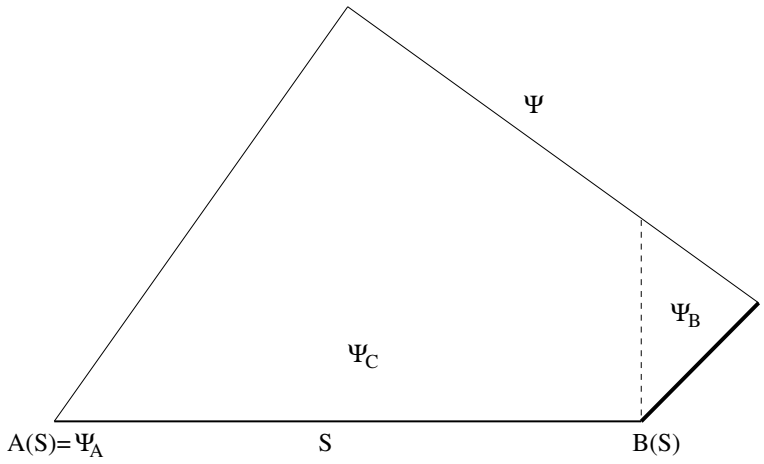


Figure 8: Decomposition of the micro–cell $\Psi$ into three subsets $\Psi_A$, $\Psi_B$, and $\Psi_C$

By the inner Voronoi tessellation, the typical cell is decomposed into a (random) number $K$ of "micro–cells", $\{\Psi^{(j)}\}_{j=1,\ldots,K}$ say, where each of these micro–cells $\Psi$ corresponds to a segment $S = S(A, B)$ of the line system $L(\Xi^*)$, whose endpoints are denoted by $A$ and $B$, respectively. This means that $S$ itself is an edge of two micro–cells.

Each micro–cell $\Psi$ is further decomposed into three non–overlapping subsets $\Psi_A$, $\Psi_B$, and $\Psi_C$, respectively; see the example given in Figure 8. In this example, we have $A(S) = \Psi_A$ and the thick line on the right is part of the boundary of the typical Voronoi cell $\Xi^*$. Moreover, the locations of lower–level components in $\Psi_B$ are connected with the endpoint $B(S)$, whereas the locations in $\Psi_C$ are projected onto $S$.

If the origin belongs to the interior of the line segment $S$, then $S$ is decomposed into two subsegments with endpoints $(A, o)$ and $(o, B)$, respectively, and $\Psi_C$ is split into two sets corresponding to these two subsegments.

Owing to the fact that for each $i = 1, \ldots, k$, the inner Voronoi tessellation completely sub-

divides the $i$th copy $\Xi_i^*$ of the typical cell into the micro–cells $\{\Psi_i^{(j)}\}_{j=1,\dots,K_i}$ and taking classical sample means, we get that $\lim_{k\to\infty} \widehat{d}_{LH}(k) = d_{LH}^*$ with probability 1, where

$$\widehat{d}_{LH}(k) = \frac{1}{\sum_{i=1}^{k} \nu_2(\Xi_i^*)} \sum_{i=1}^{k} \sum_{j=1}^{K_i} \int_{\Psi_i^{(j)}} c(P(u,o))\, du\,. \tag{4.5}$$

Notice that the expression for $\mathbb{E}_{X_L'} c(P(o,N(o)))$ given in (4.4) can be alternatively written in the form

$$\mathbb{E}_{X_L'}\, c(P(o,N(o))) = \lambda_1 \gamma\, \mathbb{E}_{X_H} \int_{\Xi^*} c(P(u,o))\, du\,. \tag{4.6}$$

Thus, if $\lambda_1$ and $\gamma$ are known, an alternative estimator $\check{d}_{LH}$ for $d_{LH}^*$ is given by

$$\check{d}_{LH}(k) = \lambda_1 \gamma\, \frac{1}{k} \sum_{i=1}^{k} \sum_{j=1}^{K_i} \int_{\Psi_i^{(j)}} c(P(u,o)\, du\,. \tag{4.7}$$

As stated in Section 2.2 we suppose in the remaining part of this paper that the cost value $c'(X_n', X_n'')$ of the "edge" with respective endpoints $X_n'$ and $X_n''$ is equal to zero. By (2.4), we then have that

$$c(P(X_n', N(X_n'))) = c(P(X_n'', N(X_n')))\,.$$

Furthermore, for the integrals appearing in (4.5) and (4.7), we have

$$\int_{\Psi_i^{(j)}} c(P(u,o)\, du = \int_{\Psi_i^{(j)}} c(P(u_p,o)\, du\,,$$

where $u_p$ denotes the closest point, seen from $u$, of the line system $L(\Xi_i^*)$ within the set $\Psi_i^{(j)}$. The following (obvious) result shows a way how these integral can be computed numerically.

**Theorem 4.2** *Let $\Psi$ be a micro–cell within the typical cell $\Xi^*$ and let $S = S(A,B)$ be the corresponding segment with endpoints $A$ and $B$, respectively, of the underlying line system $L(\Xi^*)$ restricted to $\Xi^*$. Then, with the abbreviation $c_A(S) = c(P(A,o))$ and $c_B(S) = c(P(B,o))$,*

$$\int_{\Psi} c(P(u,o))\, du = c_A(S)\nu_2(\Psi_A) + c_B(S)\nu_2(\Psi_B) + \int_{\Psi_C} c(P(u,o))\, du\,. \tag{4.8}$$

The *proof* of Theorem 4.2 immediately follows from additivity of the Lebesgue integral with respect to the domain of integration.

Notice that the first two summands on the right–hand side of (4.8) can be easily computed if Dijstra's algorithm is used in order to determine $c_A(S)$ and $c_B(S)$, respectively; see Section 5 below. With regard to computation of the third summand $f_2'(\Psi_C)$, we can proceed similarly as in the proof of formula (3.10) derived in Theorem 3.2 (cmp. Appendix B), however it might be necessary to subdivide $\Psi_C$ in order to obtain "linear functions" as integrands. Furthermore, in case $c'(X_n', X_n'') > 0$, the integrands in the integrals occuring in (4.8) have to be replaced. Then the computation is a little more challenging however not a principal problem.

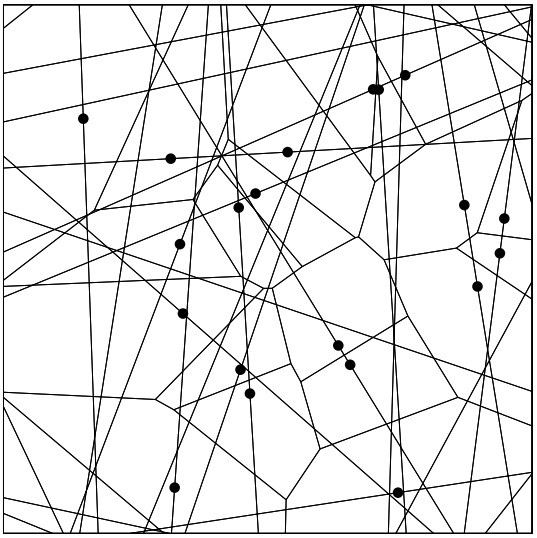

(a) *Realization of CVT and underlying lines*

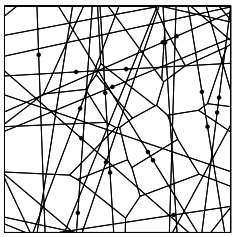

(b) *Same realization for different values of* $\lambda_1$ *and* $\gamma$ *but same quotient* $\kappa$

Figure 9: Scaling of CVT and underlying line structure

# 5 Numerial analysis

In this section we present numerical results for the two regarded network characteristics of mean shortest path length and mean subscriber line length, respectively. We start however by a brief discussion of scaling properties and run–time issues of the algorithms and by pointing out possible tests of their random outputs. Recall that in this section we assume $X_H$ to be a doubly stochastic Poisson process as pointed out in Section 2.1. Then, the whole model is completely described by the three parameters $\lambda_L$, $\lambda_1$ and $\gamma$. Besides this we assume that $c(S)$ is the length of the segment $S$, i.e. $c(S) = \nu_1(S)$. Due to the fact that in our case all cost functionals are almost surely positive, we applied Dijkstra's algorithm for the computation of shortest path lengths; see [13]. Notice that this algorithm provides both the shortetst path itself as well as its length.

## 5.1 Scaling properties of CVT

As it has already been explained in [11], with respect to the two remaining parameters $\lambda_1$ and $\gamma$, a scaling invariance property holds for any fixed value of the quotient $\kappa = \gamma/\lambda_1$. In particular suppose that $\gamma = a\gamma^{(0)}$ and $\lambda_1 = a\lambda_1^{(0)}$ for some $\gamma^{(0)}, \lambda^{(0)} > 0$, fixed and $a > 0$. Then, with respect to the typical cell $\Xi^*$ of the corresponding Voronoi tessellation, the expected number of vertices is constant, whereas the expected perimeter and the square root of the expected area of the typical cell grow linearly, proportionally to $a^{-1}$; see Figure 9.

Furthermore, the following scaling property shows that it is possible to provide estimates for the characteristics described in Sections 3 and 4 corresponding to a given parameter pair $(\gamma, \lambda_1)$ by using estimates for a different parameter pair having the same quotient $\kappa$ and by performing a suitable standardization afterwards.

**Theorem 5.1** *For any pair* $(\gamma, \lambda_1)$ *of parameters* $\gamma, \lambda_1 > 0$*, consider the (ergodic) limits* $c^*_{LH} = c^*_{LH}(\gamma, \lambda_1)$ *and* $d^*_{LH} = d^*_{LH}(\gamma, \lambda_1)$ *given in* (3.2) *and* (4.2)*, respectively. Then*

$$\gamma^{(1)}\, c^*_{LH}(\gamma^{(1)}, \lambda_1^{(1)}) = \gamma^{(2)}\, c^*_{LH}(\gamma^{(2)}, \lambda_1^{(2)}) \tag{5.1}$$

*and*

$$\gamma^{(1)}\, d^*_{LH}(\gamma^{(1)}, \lambda_1^{(1)}) = \gamma^{(2)}\, d^*_{LH}(\gamma^{(2)}, \lambda_1^{(2)}) \tag{5.2}$$

*provided that* $\gamma^{(1)}/\lambda_1^{(1)} = \gamma^{(2)}/\lambda_1^{(2)}$.

A proof of Theorem 5.1 is given in Appendix B.

## 5.2 Run–time issues

Even though it is not necessary to simulate lower–level components if we use our simulation technique as described in the previous sections, the most limiting factor with regard to run–time is the computation of shortest path lengths $c_A(S) = c(P(A(S), o))$ and $c_B(S) = c(P(B(S), o))$ by Dijkstra's algorithm. This computation has to be performed for a certain set of vertices of the underlying line system as well as for their intersection points with the boundary of $\Xi^*$ and is of order $O(n \log n)$, where $n$ is the size of the set of vertices in the corresponding graph. By this fact one can easily see that the possibility to omit the simulation of lower–level components is a huge advantage, since not only the simulation itself is no longer necessary, but also the application of Dijkstra's algorithm becomes much faster, in particular for larger values of $\lambda_2$. Notice however that, especially for large $\kappa = \gamma/\lambda_1$, run–times can become very long, because in such a case the size of the set of vertices of the graph considered above can become quite large. On the other hand, if $\kappa$ is quite small, there are few lines but relatively many higher–level points on them. From a practical viewpoint, this does not seem to be a very realistic assumption. Therefore, we restrict our investigations to $\kappa \in [10, 120]$.

## 5.3 Tests of implemented algorithms

Since outputs of our implemented algorithms are random, traditional testing procedures are not very suitable to ensure correct results. Instead, methods of testing random software have to be applied. Some examples for such tests will be mentioned in the following. For a detailed discussion of random software testing see e.g. [16]. Testing procedures for the correctness of the simulation of the typical Cox–Voronoi cell $\Xi^*$ have been discussed in detail in [11], therefore, only a short summary is given of the three different investigated methods of testing. As a first method tests using known formulae were considered, in particular it was tested if the algorithm provides correct estimates for the mean area $(\lambda_1\gamma)^{-1}$ of $\Xi^*$. As a second method the results for the algorithm were compared to results for another (already tested) algorithm and as a third method the scaling invariance property mentioned in Section 5.1 was used to construct tests for the correctness of the implemented algorithm.

Similarly, Theorem 5.1 has been used to construct tests for the mean shortest path length and the mean subscriber line length, respectively. The null–hypothesis of such tests state that (5.1) resp. (5.2) holds, where it is assumed that $\gamma^{(2)} = a\,\gamma^{(1)}$ and $\lambda_1^{(2)} = a\,\lambda_1^{(1)}$ for some $a > 0$.

All of these tests are based on classical asymptotically Gaussian distributed test statistics. The tests showed good results overall, hence we may assume that the implemented algorithm works correctly for the construction of the typical cell and the underlying line structure as wells as for the computation of the mean shortest path length and the mean subscriber line length.

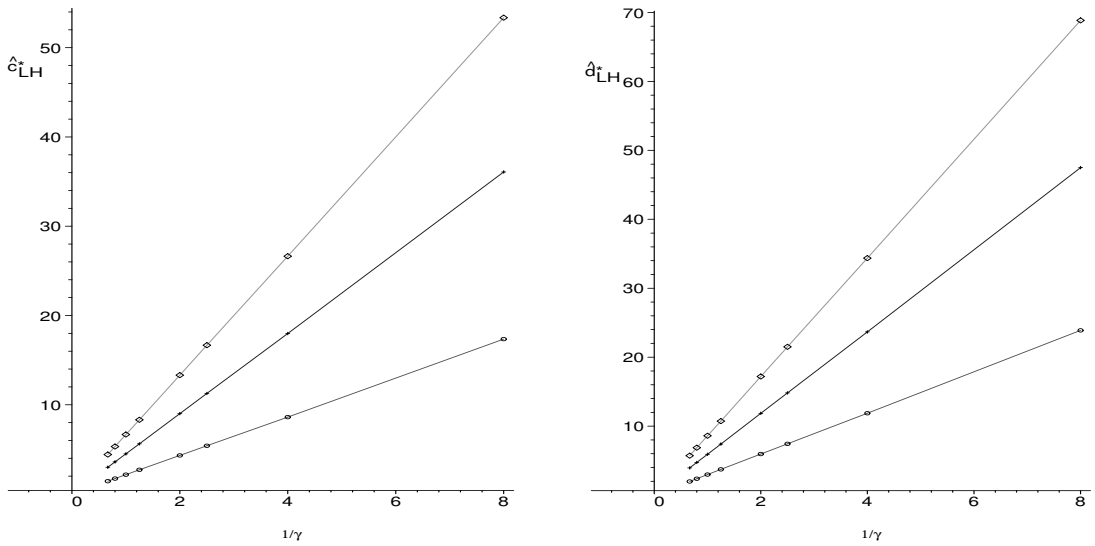


(a) *Mean shortest path length* (b) *Mean subscriber line length*

Figure 10: Network characteristics for $\kappa = 10$ (o), $\kappa = 50$ ($+$) and $\kappa = 120$ ($\diamond$)

## 5.4 Numerical results

With regard to the estimation of mean shortest path length as well as mean subscriber line length we used $k = 50000$ iterations. Figure 10 shows a visualization of the scaling invariance effect for the mean shortest path length and the mean subscriber line length (without last meter). If we take $\kappa$ to be fixed for different values of $\gamma$, then the estimated results for $c^*_{LH}$ as well as for $d^*_{LH}$ are proportional to $1/\gamma$. Therefore the graphs displayed in Figure 10 for $\kappa = 10$, $\kappa = 50$, and $\kappa = 120$ are linear and should pass through the origin. Of course, the latter property can not be directly checked since it means that $\gamma \to \infty$.

In Table 1, the corresponding estimated values for $c^*_{LH}$ and $d^*_{LH}$ are displayed. A first important observation one can make, is that for the same parameter pair $(\gamma, \lambda_1)$ we always have that $c^*_{LH} < d^*_{LH}$. If $\kappa$ increases, the quotient $c^*_{LH}/d^*_{LH}$ also slightly increases, meaning that in this case the mean shortest path length becomes larger in relation to the mean subscriber line length; see Table 2. Another interesting observation is that for both characteristics values seem to increase for increasing $\kappa$. Obviously this is due to the fact that the expected area $\mathbb{E}\nu_2(\Xi^*)$ of the typical cell $\Xi^*$ of the Cox–Voronoi tessellation also increases. Therefore it is worth looking at Table 3, where the characteristics are scaled by the square root of the expected area for the typical cell, i.e. by $(\gamma\lambda_1)^{-1/2}$. Here, the observation is that for increasing $\kappa$, the regarded quotient is decreasing for the mean shortest path length as well as for the mean subscriber line length. A possible explanation for this is that for increasing $\kappa$ and constant expected area of the typical cell, the number of lines in the typical cell increases. Therefore, with regard to mean shortest path length and mean subscriber line length, the value decreases. Another possible explanation for this is that, as it was shown in [11], the mean perimeter of the typical Cox–Voronoi cell $\Xi^*$ decreases for increasing $\kappa$ under the condition that $\mathbb{E}(\nu_2(\Xi^*))$ is kept constant. This results in typical cells being more regularly shaped in average and therefore values for the regarded functionals tend to be smaller.

Recall that by Theorem 5.1 we have

$$c^*_{LH}(\gamma, \lambda_1) = m(\kappa)\,\gamma^{-1} \tag{5.3}$$

Table 1: Estimates of mean shortest path length $c^*_{LH}$ and mean subscriber line length $d^*_{LH}$ (without last meter) for different values of $\gamma$

(a) $\kappa = 10$

| $\gamma$ | $\widehat{c}^*_{LH}$ | $\widehat{d}^*_{LH}$ |
|---|---|---|
| 0.125 | 17.355 | 23.894 |
| 0.25 | 8.615 | 11.870 |
| 0.4 | 5.409 | 7.435 |
| 0.5 | 4.323 | 5.950 |
| 0.8 | 2.711 | 3.726 |
| 1.0 | 2.169 | 2.981 |
| 1.25 | 1.727 | 2.374 |
| 1.5 | 1.440 | 1.974 |

(b) $\kappa = 50$

| $\gamma$ | $\widehat{c}^*_{LH}$ | $\widehat{d}^*_{LH}$ |
|---|---|---|
| 0.125 | 36.074 | 47.494 |
| 0.25 | 17.972 | 23.665 |
| 0.4 | 11.267 | 14.815 |
| 0.5 | 9.003 | 11.857 |
| 0.8 | 5.618 | 7.397 |
| 1.0 | 4.499 | 5.920 |
| 1.25 | 3.600 | 4.735 |
| 1.5 | 2.996 | 3.942 |

(c) $\kappa = 120$

| $\gamma$ | $\widehat{c}^*_{LH}$ | $\widehat{d}^*_{LH}$ |
|---|---|---|
| 0.125 | 53.355 | 68.841 |
| 0.25 | 26.641 | 34.360 |
| 0.4 | 16.699 | 21.502 |
| 0.5 | 13.317 | 17.191 |
| 0.8 | 8.310 | 10.723 |
| 1.0 | 6.668 | 8.609 |
| 1.25 | 5.316 | 6.865 |
| 1.5 | 4.427 | 5.710 |

Table 2: Quotient of estimated mean shortest path length $\widehat{c}^*_{LH}$ and mean subscriber line length $\widehat{d}^*_{LH}$ for different values of $\kappa$

| $\kappa$ | 10 | 20 | 30 | 40 | 50 | 60 | 90 | 120 |
|---|---|---|---|---|---|---|---|---|
| $\widehat{c}^*_{LH}/\widehat{d}^*_{LH}$ | 0.727 | 0.739 | 0.751 | 0.756 | 0.760 | 0.763 | 0.770 | 0.775 |

Table 3: Estimates of the mean shortest path length $c^*_{LH}$ and the mean subscriber line length $d^*_{LH}$ scaled by $\sqrt{\mathbb{E}(\nu_2(\Xi^*))}$

| $\kappa$ | 10 | 20 | 30 | 40 | 50 | 60 | 90 | 120 |
|---|---|---|---|---|---|---|---|---|
| $\widehat{c}^*_{LH}/\sqrt{\mathbb{E}(\nu_2(\Xi^*))}$ | 0.686 | 0.667 | 0.653 | 0.644 | 0.638 | 0.632 | 0.617 | 0.609 |
| $\widehat{d}^*_{LH}/\sqrt{\mathbb{E}(\nu_2(\Xi^*))}$ | 0.944 | 0.903 | 0.870 | 0.852 | 0.840 | 0.828 | 0.801 | 0.786 |

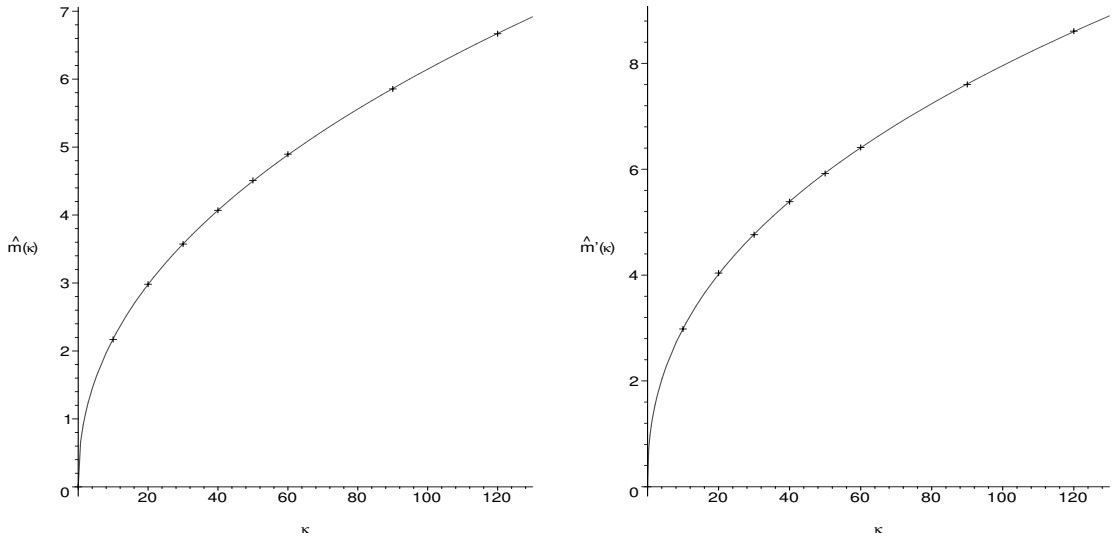


(a) *Mean shortest path length* (b) *Mean subscriber line length*

Figure 11: Estimates for the slopes $m(\kappa)$ and $m'(\kappa)$ for different $\kappa$ and the fitted function

and

$$d^*_{LH}(\gamma, \lambda_1) = m'(\kappa)\, \gamma^{-1}\,, \tag{5.4}$$

where $m(\kappa)$ and $m'(\kappa)$ are constants depending only on the quotient $\kappa = \gamma/\lambda_1$. If we return to the graphs displayed in Figure 10, we can obtain the estimates $\widehat{m}(\kappa)$ and $\widehat{m}'(\kappa)$ for the slopes $m(\kappa)$ and $m'(\kappa)$ of the lines for $\kappa$ constant and $1/\gamma$ variable.

The knowledge of $\widehat{m}(\kappa)$ and $\widehat{m}'(\kappa)$ thereby leads to the possibility of estimating the mean shortest path length and the mean subscriber line length without having to do simulations for any given parameter pair $(\gamma, \lambda_1)$, since then, only these parameter values need to be plugged into (5.3) and (5.4) to obtain estimates for $c^*_{LH}$ and $d^*_{LH}$. Computationally these slopes are estimated for certain discrete values of $\kappa$ and subsequently a function is fitted using the measurement points. Figure 11 displays some values of estimated slopes as well as a fitted function. Regarding the estimated values we used

$$m(\kappa) = a\kappa^b \qquad \text{and} \qquad m'(\kappa) = a'\kappa^{b'}\,,$$

where $a, a\prime \in \mathbb{R}$ and $b, b' \in (0, 1]$. Using the least squares method we obtained $a = 0.7739$, $b = 0.450$ and $a' = 1.1242$, $b' = 0.425$. For applications this induces an easy way to compute mean shortest path lengths and mean subscriber lengths without performing any furter simulations. For example, if we take the two model parameters to be $\gamma = 2$ (mean length of the line system per unit area) and $\lambda_1 = 0.04$ (mean number of higher–level points per unit area) we directly obtain esimates $\widehat{m}(50) = 4.5001$ and $\widehat{m}'(50) = 5.9280$ that lead to estimates for $c^*_{LH}(\gamma, \lambda_1)$ and $d^*_{LH}(\gamma, \lambda_1)$ given by 2.2501 and 2.9640, respectively.

# 6 Discussion and outlook

In this paper we presented efficient techniques for the estimation of mean shortest path length and mean subscriber line length in two-level hierarchical models, using Monte Carlo simulation. In particular, the formulae given in Section 5.4 provide a fast and efficient way

to precisely estimate these characteristics without performing any further simulations for any pair of model parameters $\gamma, \lambda_1$. Apart from the numerical results, certainly of interest in their own right, the techniques introduced in this paper are useful for the simulation and estimation of similar characteristics for more sophisticated models. In this context we would like to mention some different possible extensions.

First of all, often the distribution (additionally to the expectation) of the mean shortest path length and mean subscriber line length, respectively, are of interest. This might for example be useful with respect to a risk analysis based on tail probabilities. Notice that distributions for these characteristics can be obtained in a very similar fashion compared to expectations, thereby recycling most of the tools given here.

Secondly, in some cases there might arise a need of extending the underlying geometry model, since, depending on real data, sometimes other tessellation models or models that are more complicated, like iterated tessellations, might be a better choice for an underlying geometry model as the Poisson line tessellations regarded here. Especially in the case of iterated tessellations ([15]) whose initial tessellations are of Poisson line type, our simulation techniques of the network characteristics demand only slight adaption. For other tessellation types, further modifications are needed, but notice that the computation formulae for network characteristics still hold as long as the placement of network components is performed using Poisson processes. Hence, regarding these aspects, no modifications have to be done.

Finally it might be of interest to regard more than two levels of hierarchy. At least approximative formulae can be provided in the case of such multi–level models. If there is a need to be more exact, the simulation of the components of the different levels might become necessary. In the context of cost analysis by using simulation studies, and regarding the fact that the associated software becomes more and more complex, the topic of random software tests, as it was briefly mentioned in Section 5 will become more and more important. With regard to the algorithms used throughout this paper, we performed a lot of test series in order to be quite sure that our algorithms are correctly implemented.

In summary, we think that the topics described in this paper, together with the techniques described in [12] for fitting random tessellation models to real data are a first step towards an efficient and fast cost analysis tool for telecommunication access networks, based on models of random geometry.

*Acknowledgements.* This research was supported by France Télécom R&D through research grant No. 42 36 68 97. The authors are grateful to Michael Rösch for his help in performing the simulations, which lead to the numerical results.

# References

[1] F. Baccelli and B. Blaszczyszyn (2001). On a coverage process ranging from the Boolean model to the Poisson-Voronoi tessellation. *Advances in Applied Probability* **33**, 293–323.

[2] F. Baccelli, C. Gloaguen, and S. Zuyev (2000). Superposition of Planar Voronoi Tessellations. *Communications in Statistics, Series Stochastic Models* **16**, 69–98.

[3] F. Baccelli, M. Klein, M. Lebourges, and S. Zuyev (1996). Géométrie aléatoire et architecture de réseaux. *Annales des Télécommunication* **51**, 158–179.

[4] F. Baccelli, D. Kofman, and J.L. Rougier (1999). Self organizing hierarchical multicast trees and their optimization. *Proceedings of IEEE Infocom '99*, 1081–1089, New York.

[5] F. Baccelli and S. Zuyev (1996). Poisson-Voronoi spanning trees with applications to the optimization of communication networks. *Operations Research* **47**, 619–631.

[6] B. Błaszczyszyn and R. Schott (2003). Approximate decomposition of some modulated Poisson–Voronoi tessellations. *Advances in Applied Probability* **35**, 847-862.

[7] B. Błaszczyszyn and R. Schott (2005). Approximations of functionals of some modulated Poisson–Voronoi tessellations with applications to modeling of communication networks. *Japan Journal of Industrial and Applied Mathematics*, **22**(2), 179–204.

[8] D.J. Daley and D. Vere-Jones (1988). *An Introduction to the Theory of Point Processes.* Springer, New York.

[9] R. Diestel (1997). *Graph Theory.* Springer, New York.

[10] C. Gloaguen, P. Coupé, R. Maier and V. Schmidt (2002). Stochastic modelling of urban access networks. In *Proc. 10th Internat. Telecommun. Network Strategy Planning Symp.* (Munich, June 2002), VDE, Berlin, 99–104.

[11] C. Gloaguen, F. Fleischer, H. Schmidt and V. Schmidt (2005). Simulation of typical Cox-Voronoi cells with a special regard to implementation tests. *Mathematical Methods of Operations Research* **62**(3), 357–373.

[12] C. Gloaguen, F. Fleischer, H. Schmidt and V. Schmidt (2006). Fitting of stochastic telecommunication network models, via distance measures and Monte-Carlo tests. *Telecommunication Systems* **31**, 353–377.

[13] D. Jungnickel (1997). *Graphs, Networks and Algorithms.* Springer, Berlin.

[14] R. Maier (2003). *Iterated Random Tessellations with Applications in Spatial Modelling of Telecommunication Networks.* Doctoral Dissertation, University of Ulm.

[15] R. Maier and V. Schmidt (2003). Stationary iterated tessellations. *Advances in Applied Probability* **35**, 337–353.

[16] J. Mayer and R. Guderlei (2004). Test oracles and randomness. *Lecture Notes in Informatics* P-58:179–189, Köllen Druck+Verlag GmbH, Bonn.

[17] J. Mayer, V. Schmidt and F. Schweiggert (2004). A unified simulation framework for spatial stochastic models. *Simulation Modelling Practice and Theory* **12**, 307–326.

[18] M. Miyazawa (1995). Note on generalizations of Mecke's formula and extensions of $H = \lambda G$. *Journal of Applied Probability* **32**, 105–122.

[19] J. Neveu (1976). Processus ponctuels. In A. Dold and B. Eckman (eds): *Lecture Notes in Mathematics* **598**, Springer, Berlin, 249–445.

[20] R. Schneider and W. Weil (2000). *Stochastische Geometrie.* Teubner, Stuttgart.

[21] R. Serfozo (1999). *Introduction to Stochastic Networks*, Springer, Berlin.

[22] D. Stoyan, W.S. Kendall and J. Mecke (1995). *Stochastic Geometry and its Applications.* 2nd ed., J. Wiley & Sons, Chichester.

[23] K. Tchoumatchenko and S. Zuyev (2001). Aggregate and fractal tessellations. *Probability Theory Related Fields* **121**, 198–218.

# A Mathematical background

In this section, the basic notation used in the present paper is introduced. Furthermore, we briefly explain the notions and some properties of random point processes and random tessellations, serving as models for the network components and for the network geometry, respectively. The notions of graphs and shortest paths are also mentioned. For a more detailed discussion of the topics mentioned here, the reader is referred to [9], [13], [19], [20], and [22], for example.

## A.1 Basic notations

In the following, let $\mathbb{R}$ be the set of real numbers and let $\mathbb{N}$ be the set of positive integers, which is extended by $\mathbb{N}_0 = \mathbb{N} \cup \{0\}$ to the set of all non–negative integers.

The abbreviations $\operatorname{int} B, \partial B$, and $B^c$ are used to denote the interior, the boundary, and the complement of a set $B \subset \mathbb{R}^2$, respectively, where $\mathbb{R}^2$ denotes the 2–dimensional Euclidean space. For any vector $x = (x_1, x_2)$ in $\mathbb{R}^2$ we define the Euclidean norm $||.|| : \mathbb{R}^2 \to [0, \infty)$ by

$$||x|| = \left(x_1^2 + x_2^2\right)^{1/2}. \tag{A.1}$$

Furthermore, $B_r(x)$ and $B_r^{\neq}(x)$ denote, respectively, the 2–dimensional closed and open ball centered at $x \in \mathbb{R}^2$ with radius $r > 0$, i.e. $B_r(x) = \{y \in \mathbb{R}^2 : ||x-y|| \leq r\}$ and $B_r^{\neq}(x) = \{y \in \mathbb{R}^2 : ||x-y|| < r\}$.

On $\mathbb{R}^2$ we define two topological groups, namely the group $t_x : y \mapsto y + x$ of all translations for $x \in \mathbb{R}^2$ and the group $\vartheta_R : y \mapsto Ry$ of all rotations around the origin, where $R$ denotes a $2 \times 2$–matrix, orthogonal and with $\det R = 1$. This allows us to introduce the following operations on sets $B \subset \mathbb{R}^2$, the translation $t_x B = \{y + x : y \in B\}$ for $x \in \mathbb{R}^2$ and the rotation $\vartheta_R B = \{\vartheta_R x : x \in B\}$ around the origin $o$, respectively.

Furthermore, we introduce the families of all closed sets, compact sets, and convex bodies (compact and convex sets) in $\mathbb{R}^2$, denoted by $\mathcal{F}$, $\mathcal{K}$, and $\mathcal{C}$, respectively.

Recall that $(\mathbb{R}^2, \mathcal{B}(\mathbb{R}^2))$ is a measurable space with $\mathcal{B}(\mathbb{R}^2)$ denoting the family of Borel sets of the $\mathbb{R}^2$. Furthermore, let $\mathcal{B}_0(\mathbb{R}^2)$ denote the family of all bounded Borel sets in $\mathbb{R}^2$. Two prominent examples of measures acting on $(\mathbb{R}^2, \mathcal{B}(\mathbb{R}^2))$ are given by the (2–dimensional) Lebesgue measure $\nu_2 : \mathcal{B}(\mathbb{R}^2) \to [0, \infty]$, where we may interpret $\nu_2(B)$ as area of $B$ for any Borel set $B \in \mathcal{B}(\mathbb{R}^2)$, and by (locally finite) counting measures $\varphi$ on $(\mathbb{R}^2, \mathcal{B}(\mathbb{R}^2))$, respectively, where the latter measures can be expressed by the (countable) sum $\varphi = \sum_{i=1}^{n} \delta_{x_i}$ for $n \in \mathbb{N}_0 \cup \{\infty\}$. Here, for $x \in \mathbb{R}^2$ and $B \in \mathcal{B}(\mathbb{R}^2)$ we call the probability measure $\delta_x(B) = \mathbb{1}_B(x)$ on $(\mathbb{R}^2, \mathcal{B}(\mathbb{R}^2))$ the Dirac measure. Notice that any $x \in \mathbb{R}^2$ is called an atom of the counting measure $\varphi$ if $\varphi(\{x\}) > 0$. Moreover $\varphi$ is called simple if $\varphi(\{x\}) \in \{0, 1\}$ for $x \in \mathbb{R}^2$ and locally finite if for any compact set $K \in \mathcal{K}$ we have that $\varphi(K) < \infty$. In the sequel we will consider only the set of simple and locally finite counting measures and therefore we will denote this set by $M = M(\mathbb{R}^2)$ equipped with the $\sigma$–algebra $\mathcal{M} = \mathcal{M}(\mathbb{R}^2)$, which is the smallest $\sigma$–algebra of subsets of $M(\mathbb{R}^2)$ containing all sets of the form $\{\varphi \in M(\mathbb{R}^2) : \varphi(B) = j\}$, where $j \in \mathbb{N}_0$ and $B \in \mathcal{B}_0(\mathbb{R}^2)$.

The support of $\varphi$ is the set $\operatorname{supp}(\varphi) = \{x \in \mathbb{R}^2 : \varphi(\{x\}) > 0\}$, which is locally finite itself if $\varphi$ is locally finite. Also we introduce the shift operator $t_x : M(\mathbb{R}^2) \to M(\mathbb{R}^2)$ defined by $t_x\varphi(B) = \varphi(t_x^{-1}B) = \varphi(t_{-x}B)$ for $x \in \mathbb{R}^2$ as well as the rotation operator $\vartheta_R : M(\mathbb{R}^2) \to M(\mathbb{R}^2)$ by $\vartheta_R\varphi(B) = \varphi(\vartheta_R^{-1}B) = \varphi(\vartheta_{R^{-1}}B)$ for any rotation $R$ around the origin.

Recall that a random closed set $\Xi$ in $\mathbb{R}^2$ is a measurable mapping $\Xi : \Omega \to \mathcal{F}$ from some probability space $(\Omega, \mathcal{A}, \mathbb{P})$ into the measurable space $(\mathcal{F}, \mathcal{B}(\mathcal{F}))$, where $\mathcal{B}(\mathcal{F})$ denotes the smallest $\sigma$–algebra of subsets of $\mathcal{F}$ that contains all sets $\{F \in \mathcal{F}, F \cap K \neq \emptyset\}$ for any $K \in \mathcal{K}$. Particularly, the random closed set $\Xi$ is called a random compact set or a random convex body if $\mathbb{P}(\Xi \in \mathcal{K}) = 1$ or $\mathbb{P}(\Xi \in \mathcal{C}) = 1$, respectively.

## A.2 Planar point processes

**Definition**
A *random point process* $X$ in $\mathbb{R}^2$ is a measurable mapping $X : \Omega \to M$ from some probability space $(\Omega, \mathcal{A}, \mathbb{P})$ into the measurable space $(M, \mathcal{M})$, i.e. one way of looking at point processes is to regard them as counting measures $\sum_{x \in \operatorname{supp}(X)} \delta_x$ and, hence, interpreting $X(B)$ as the (random) number of points of $X$ in $B \in \mathcal{B}(\mathbb{R}^2)$. Notice that we can also identify a point process $X$ with its support $\operatorname{supp}(X)$ and, hence, get an alternative interpretation of $X$ as a (planar) random closed set. Moreover, it is sometimes also convenient to write $X = \{X_n\}_{n \geq 1}$, which expresses $X$ as a sequence $X_1, X_2, \ldots$ of random vectors $X_n : \Omega \to \mathbb{R}^2$ for $n \geq 1$.

**Basic properties**
The distribution of $X$ is denoted by $\mathbb{P}_X$ and defined by $\mathbb{P}_X(A) = \mathbb{P}(X \in A)$ for $A \in \mathcal{M}$. We call the point process $X$ stationary if $\mathbb{P}_X = \mathbb{P}_{t_x X}$ for any $x \in \mathbb{R}^2$, i.e. if the shifted process $t_x X$ has the same distribution as the original $X$. Moreover $X$ is called isotropic, if $\mathbb{P}_X = \mathbb{P}_{\vartheta_R X}$ for any rotation $\vartheta_R$ around the origin, i.e. if the distribution of the rotated process $\vartheta_R X$ coincides with the distribution of the original process.

**Intensity measure**
The *intensity measure* $\Lambda : \mathcal{B}(\mathbb{R}^2) \to [0, \infty]$ of a point process $X$ is defined by

$$\Lambda(B) = \mathbb{E}X(B)\,, \quad B \in \mathcal{B}(\mathbb{R}^2)\,, \tag{A.2}$$

i.e., $\Lambda(B)$ is the expected number of points of $X$ in $B$. If $X$ is stationary and $\Lambda$ is not equal to the zero measure, it can be shown that $\Lambda(B) = \lambda \nu_2(B)$, where $\lambda > 0$ is called the *intensity* of $X$ and can be interpreted as the expected number of points per unit area, i.e. $\lambda = \mathbb{E}X((0,1]^2)$.

**Poisson point processes**
Let $X$ be a point process in $\mathbb{R}^2$, fulfilling

$$\mathbb{P}(X(B) = k) = e^{-\Lambda(B)} \frac{\Lambda(B)^k}{k!}\,, \quad B \in \mathcal{B}_0(\mathbb{R}^2)\,, k \in \mathbb{N}_0\,, \tag{A.3}$$

then $X$ is called *Poisson point process* with intensity measure $\Lambda$.

## A.3 Planar marked point processes

**Definition**
Marked point processes can be seen as a generalization of point processes, where each point is additionally equipped with a mark taken from some mark space $D$. More technically, one assumes $D$ to be a so–called Polish space and denotes by $\mathcal{B}(D)$ the $\sigma$–algebra of its Borel sets. Let $M_D = M(\mathbb{R}^2 \times D)$ be the set of all measures $\psi : \mathcal{B}(\mathbb{R}^2) \times \mathcal{B}(D) \to \mathbb{N}_0 \cup \{\infty\}$ which are simple and locally finite in the first component, i.e., each $\psi \in M_D$ can be represented as

$$\psi(B \times G) = \sum_{[x,m] \in \mathrm{supp}(\psi)} \delta_{[x,m]}(B \times G)\,. \tag{A.4}$$

Finally, let $\mathcal{M}_D = \mathcal{M}(\mathbb{R}^2 \times D)$ be the smallest $\sigma$–algebra of subsets of $M_D$ containing all sets of the form $\{\psi \in M_D : \psi(B \times G) = j\}$ for $B \in \mathcal{B}_0(\mathbb{R}^2)$, $G \in \mathcal{B}(D)$ and $j \in \mathbb{N}_0$. Then, the mapping $X_D : \Omega \to M_D$ from $(\Omega, \mathcal{A}, \mathbb{P})$ into $(M_D, \mathcal{M}_D)$ is called *random marked point process* in $\mathbb{R}^2$ with mark space $(D, \mathcal{B}(D))$ and can be represented analogously to (A.4).

**Basic properties**
The distribution of $X_D$ is denoted by $\mathbb{P}_{X_D}$ and defined by $\mathbb{P}_{X_D}(A) = \mathbb{P}(X_D \in A)$ for $A \in \mathcal{M}_D$. Again, it is often convenient to consider alternative representations of $X_D$, for example the representation as a collection of random marked points, expressed by $X_D = \{[X_n, D_n]\}_{n \geq 1}$, where both $X_n : \Omega \to \mathbb{R}^2$ and $D_n : \Omega \to D$ are measurable mappings. $X_D$ is called independently marked if $\{X_n\}_{n \geq 1}$ and $\{D_n\}_{n \geq 1}$ are independent and beyond that $\{D_n\}_{n \geq 1}$ consists of independent and identically distributed random variables. Stationarity and isotropy are now introduced with respect to the first component of the marked point process $X_D$, i.e. $X_D$ is stationary if $X_D \stackrel{d}{=} \{[t_x X_n, D_n]\}$ for all $x \in \mathbb{R}^2$ and isotropic if $X_D \stackrel{d}{=} \{[\vartheta_R X_n, D_n]\}$ for all rotations $\vartheta_R$ around the origin, where $\stackrel{d}{=}$ denotes equality in distribution.

**Intensity measure**
The *intensity measure* $\Lambda_D : \mathcal{B}(\mathbb{R}^2) \times \mathcal{B}(D) \to [0, \infty]$ of a marked point process $X_D$ is defined by

$$\Lambda_D(B \times G) = \mathbb{E}X_D(B \times G)\,, \quad B \in \mathcal{B}(\mathbb{R}^2)\,, G \in \mathcal{B}(D)\,, \tag{A.5}$$

i.e., $\Lambda_D(B \times G)$ is the expected number of points of $X_D$ in $B$ with a mark in $G$. In case of stationarity, analogous to stationary non–marked point processes, the intensity measure $\Lambda_D$ admits the decomposition (see [20], p. 89)

$$\Lambda_D(B \times G) = \lambda \int_{\mathbb{R}^2} \int_D \mathbb{1}_B(x)\, \mathbb{1}_G(m) P(dm) dx\,, \quad B \in \mathcal{B}(\mathbb{R}^2)\,, G \in \mathcal{B}(D)\,, \tag{A.6}$$

where $\lambda > 0$ is again called intensity and $P : \mathcal{B}(D) \to [0,1]$ is the Palm mark distribution of $X_D$, given by

$$P(G) = \frac{1}{\lambda \nu_2(B)}\, \mathbb{E} \sum_{[x,m] \in \mathrm{supp}(X_D)} \mathbb{1}_B(x)\, \mathbb{1}_G(m)\,, \quad G \in \mathcal{B}(D)\,, \tag{A.7}$$

for any $B \in \mathcal{B}(\mathbb{R}^2)$ with $0 < \nu_2(B) < \infty$.

## A.4 Neveu's exchange formula

In the following we present Neveu's exchange formula adapted to (marked) point process in $\mathbb{R}^2$. To capture the randomness inherent in such a system of several random processes, we consider a so–called *flow* $\{\theta_x : x \in \mathbb{R}^2\}$ on the space $\Omega$, i.e. a family of bijective shift operators $\theta_x : \Omega \to \Omega$ such that $\theta_x \circ \theta_y = \theta_{x+y}$, where $\circ$ denotes the concatenation operator. Furthermore, we assume that the mapping $f : \mathbb{R}^2 \times \Omega \to \Omega$ with $f(x,\omega) = \theta_x \omega$ is measurable. For $x \in \mathbb{R}^2$ we assume that $\theta_x$ is compatible with our shift operator $t_x$ as defined in Section A.1, which means that

$$X_D(\theta_x \omega, B \times G) = t_x X_D(\omega, B \times G) = X_D(\omega, t_{-x} B \times G)\,, \tag{A.8}$$

for any marked point process $X_D : \Omega \to M_D$ and all $B \in \mathcal{B}(\mathbb{R}^2)$, $G \in \mathcal{B}(D)$. Notice that then we can get the stationarity of $X_D$ by assuming that

$$\mathbb{P}(\theta_x A) = \mathbb{P}(\theta_x^{-1} A) = \mathbb{P}(A)\,, \tag{A.9}$$

for all $A \in \mathcal{A}$ and $x \in \mathbb{R}^2$, where $\theta_x A = \{\theta_x \omega : \omega \in A\}$.

Also, using the definition of the operator $\theta_x$, we introduce the Palm distribution $\mathbb{P}^{(o)}_{X_D}$ for a stationary marked point process $X_D$ as the probability measure $\mathbb{P}^*_{X_D}$ on $\mathcal{A} \otimes \mathcal{B}(D)$ by

$$\mathbb{P}^*_{X_D}(A \times G) = \frac{1}{\lambda \nu_2(B)} \int_\Omega \int_{\mathbb{R}^2 \times G} \mathbb{1}_B(x)\, \mathbb{1}_A(\theta_x \omega)\, X(\omega, d(x,g)) \mathbb{P}(d\omega) \tag{A.10}$$

for any $B \in \mathcal{B}(\mathbb{R}^2)$ with $0 < \nu_2(B) < \infty$.

**Theorem A.1** (Neveu's exchange formula) *Let $X_D$ and $\widetilde{X}_{\widetilde{D}}$ be arbitrary stationary marked point processes on $\mathbb{R}^2$ with mark spaces $D$ and $\widetilde{D}$ and intensities $\lambda$ and $\widetilde{\lambda}$, respectively. Then, for any measurable function $f : \mathbb{R}^2 \times D \times \widetilde{D} \times \Omega \to [0,\infty)$,*

$$\begin{aligned} &\lambda \int_{\Omega \times D} \int_{\mathbb{R}^2 \times \widetilde{D}} f(x, g, \widetilde{g}, \theta_x \omega) \widetilde{X}_{\widetilde{D}}(\omega, d(x, \widetilde{g})) \mathbb{P}^*_{X_D}(d(\omega, g)) \\ &\quad = \widetilde{\lambda} \int_{\Omega \times \widetilde{D}} \int_{\mathbb{R}^2 \times D} f(-x, g, \widetilde{g}, \omega) X_D(\omega, d(x, g)) \mathbb{P}^*_{\widetilde{X}_{\widetilde{D}}}(d(\omega, \widetilde{g}))\,. \end{aligned} \tag{A.11}$$

## A.5 Poisson line processes

Consider the space $\mathcal{S}$ of all affine 1–dimensional subspaces (lines) in $\mathbb{R}^2$ and let $\mathcal{L} = \{L \in \mathcal{S} : o \in L\}$. A point process $X$ in $\mathcal{F}' = \mathcal{F} \setminus \{\emptyset\}$ is called a (planar) *line process* if for the intensity measure $\Lambda$ of $X$ it holds that $\Lambda(\mathcal{F}' \setminus \mathcal{S}) = 0$. In case of stationarity, $\Lambda$ can be disintegrated as follows. Suppose

that $\Lambda$ is locally finite and not equal to the zero measure. Then, there exists a constant $\lambda_\ell \in (0,\infty)$ and a probability measure $\Theta$ on $\mathcal{B}(\mathcal{L})$, called the *orientation distribution* of $X$, such that

$$\Lambda(B) = \lambda_\ell \int_{\mathcal{L}} \int_{L^\perp} \mathbb{1}_B(L+x)\nu_1(dx)\Theta(dL) \tag{A.12}$$

for any $B \in \mathcal{B}(\mathcal{S})$, where $\nu_1$ denotes the 1–dimensional Lebesgue–measure on the orthogonal complement $L^\perp \in \mathcal{L}$ of $L \in \mathcal{L}$. In order to interpret the constant $\lambda_\ell$ we note that (A.12) yields

$$\lambda_\ell = \frac{1}{2}\,\mathbb{E}X(L \in \mathcal{S} : L \cap B_1(o) \neq \emptyset)\,. \tag{A.13}$$

Hence $2\lambda_\ell$ is the expected number of lines hitting the unit ball $B_1(o)$ centered at the origin and with radius 1. In particular, we consider the case of $X$ being a stationary and isotropic Poisson line process. Then, $X$ can be represented in the form $X = \sum_{n\geq 1} \delta_{\ell_{(R_n,V_n)}}$, where $\{R_n\}$ is a stationary Poisson point process in $[0,\infty)$ with intensity $\lambda_\ell$ and where $\{V_n\}$ is an independent sequence of independent and identically distributed random variables with uniform distribution on $[0, 2\,\pi)$. For each line $\ell_{(R_n,V_n)}$, the angle $V_n$ is measured in anti–clockwise direction between the positive $x$–axis and the outer orientation vector of the line, whereas $R_n$ denotes the perpendicular distance of the line to the origin. Notice that (A.12) can be written as

$$\Lambda(B) = \frac{\lambda_\ell}{2\,\pi} \int_0^{2\pi} \int_0^{\infty} \mathbb{1}_B(\ell_{(r,v)})drdv\,, \qquad B \in \mathcal{B}(\mathcal{S})\,. \tag{A.14}$$

Furthermore, each line $\ell_{(R_n,V_n)}$ in $\mathbb{R}^2$ can be described by its Hessian normal form $\ell_{(R_n,V_n)} = \{(x,y) \in \mathbb{R}^2 : x\cos V_n + y \sin V_n = R_n\}$. It is easy to see that the expected total length $\mathbb{E}\sum_{n\geq 1} \nu_1(\ell_{(R_n,V_n)} \cap B_1(o))$ of lines $\ell_{(R_n,V_n)}$ in the unit ball $B_1(o)$ is given by $\pi\lambda_\ell$. Thus, $\gamma = \lambda_\ell$ is the expected total length per unit area and called the *intensity* of the random closed set $X_\ell = \bigcup_{n\geq 1} \ell_{(R_n,V_n)}$. For simplicity, both $X_\ell$ and $X = \sum_{n\geq 1} \delta_{\ell_{(R_n,V_n)}}$ are called Poisson line processes; see also Fig. 2(a).

## A.6 Cox processes induced by Poisson line processes

In order to describe (doubly stochastic) point processes in $\mathbb{R}^2$ located on the lines of Poisson line processes, we use the concept of *Cox processes*. Such processes can be seen as a generalization of (inhomogeneous) Poisson point processes in $\mathbb{R}^2$. More formally, let $X_\ell$ be a stationary and isotropic Poisson line process with intensity $\gamma$. Then, given $X_\ell$, the Cox process $X_c$ is a Poisson point process in $\mathbb{R}^2$ with (conditional) intensity measure $\Lambda_c(\cdot \mid X_\ell) = \lambda\nu_1(X_\ell \cap \cdot)$ for some $\lambda > 0$. In particular, $X_c$ is a stationary and isotropic point process in $\mathbb{R}^2$ whose intensity measure $\Lambda_c$ satisfies the relationships

$$\Lambda_c(\cdot) = \mathbb{E}X_c(\cdot) = \lambda\mathbb{E}\nu_1(X_\ell \cap \cdot) = \lambda_c\nu_2(\cdot)\,, \tag{A.15}$$

where $\lambda_c = \lambda\gamma$ is the intensity of $X_c$. Furthermore, the point processes on the individual lines of the Poisson line process $X_\ell$ are (1–dimensional) Poisson point processes with intensity $\lambda$. Thus, $\lambda$ can be interpreted as mean number of points per unit length of $X_\ell$. In Fig. 2(b), a realization of a Cox process is shown, induced by Poisson point processes on the lines of a Poisson line process.

## A.7 Cox–Voronoi tessellations and typical cells

**Planar tessellations**

A *tessellation* in $\mathbb{R}^2$ is a countable family $\tau = \{C_n\}_{n\geq 1}$ of convex bodies $C_n \in \mathcal{C}$ such that $\operatorname{int} C_n \neq \emptyset$ for all $n$, $\operatorname{int} C_n \cap \operatorname{int} C_m = \emptyset$ for all $n \neq m$, $\bigcup_{n\geq 1} C_n = \mathbb{R}^2$, and $\sum_{n\geq 1} \mathbb{1}_{\{C_n \cap K \neq \emptyset\}} < \infty$ for any $K \in \mathcal{K}$. Notice that the sets $C_n$, called the *cells* of $\tau$, are polygons in $\mathbb{R}^2$. The family of all tessellations in $\mathbb{R}^d$ is denoted by $\mathcal{T}$. A *random tessellation* $\{\Xi_n\}_{n\geq 1}$ in $\mathbb{R}^d$ is a sequence of random convex bodies $\Xi_n$ such that $\mathbb{P}(\{\Xi_n\}_{n\geq 1} \in \mathcal{T}) = 1$. Notice that a random tessellation $\{\Xi_n\}_{n\geq 1}$ can also be considered as a marked point process $\sum_{n\geq 1} \delta_{[\alpha(\Xi_n),\Xi_n^o]}$, where $\alpha : \mathcal{C}' \to \mathbb{R}^d$, $\mathcal{C}' = \mathcal{C} \setminus \{\emptyset\}$, is a measurable mapping such that $\alpha(C) \in C$ and $\alpha(C+x) = \alpha(C) + x$ for any $C \in \mathcal{C}'$ and $x \in \mathbb{R}^d$,

and where $\Xi_n^o = \Xi_n - \alpha(\Xi_n)$ is the centered cell corresponding to $\Xi_n$ which contains the origin. The point $\alpha(C) \in \mathbb{R}^d$ is called the associated point of $C$ and can be chosen, for example, to be the lexicographically smallest point of $C$.

**Poisson line tessellations and induced tessellations**
A *Poisson line tessellation* (PLT) is induced by a random Poisson line process $X_\ell$ in $\mathbb{R}^2$ which itself can be interpreted as an independently marked Poisson process on $[0,\infty) \times [0, 2\,\pi]$. Generally, the intensity $\gamma_{PLT}$ of a PLT coincides with the intensity of its generating Poisson line process (see Section A.5) and, hence, can be interpreted as mean total length of edges per unit area. Based on the doubly stochastic point process $X_c$ defined in Section A.6, a Cox-Voronoi tessellation can easily be introduced by applying the nearest-neighbor principle to this type of point process; see Fig. 2(c).

**Typical cell and zero cell of stationary tessellations**
Suppose that the marked point process $X_\tau = \sum_{n\geq 1} \delta_{[\alpha(\Xi_n), \Xi_n^0]}$ is stationary with positive and finite intensity $\lambda_\tau = \mathbb{E}\#\{n : \alpha(\Xi_n) \in [0,1)^2\}$. By $\mathcal{P}^o$ we denote the family of all convex polytopes with their associated point at the origin. Then, the *Palm mark distribution* $\mathbb{P}_{X_\tau}^{(o)}$ of $X_\tau$ is given by $\mathbb{P}_{X_\tau}^{(o)}(B) = \lambda_\tau^{-1}\, \mathbb{E}\#\{n : \alpha(\Xi_n) \in [0,1)^2, \Xi_n^o \in B\}$ for any $B \in \mathcal{B}(\mathcal{F}) \cap \mathcal{P}^o$. Notice that a random polytope $\Xi^* : \Omega \to \mathcal{P}^o$, whose distribution coincides with $\mathbb{P}_{X_\tau}^{(o)}$, is called the *typical cell* of $X_\tau$. Furthermore, it holds that

$$\lambda_\tau^{-1} = \int_{\mathcal{P}^0} \nu_2(C)\, \mathbb{P}_{X_\tau}^{(o)}(dC)\,, \tag{A.16}$$

i.e., the expected area $\mathbb{E}\nu_2(\Xi^*) = \int_{\mathcal{P}^o} \nu_2(C)\, \mathbb{P}_{X_\tau}^{(o)}(dC)$ of the typical cell $\Xi^*$ is equal to $\lambda_\tau^{-1}$.

## A.8 Graphs and shortest paths

A *graph* is a pair $G = (V, E)$ of sets that satisfies $E \subset [V]^2$, which means that the elements of $E$ are 2-element subsets of the finite set $V$, which contains at least two elements. The elements of $V$ are called *vertices* of the graph $G$, while the elements of $E$ are its *edges*. With respect to a set of edges $E$, a cost function $c : E \to [0,\infty)$ can be defined that assigns to each edge $e \in E$ a cost value $c(e)$, for example its Euclidean length if $v \in \mathbb{R}^2$ for all $v \in V$. A subgraph $P$ with a vertex set $V_P = \{v_0, v_1, ..., v_k\}$ and edge set $E_P = \{v_0v_1, v_1v_2, ..., v_{k-1}v_k\}$ is called a *path* from the *initial vertex* $v_0$ to the *terminal vertex* $v_k$. If a corresponding cost function $c$ is given, the *(weighted) path length* is defined by

$$c(P) = \sum_{i=1}^{k} c(v_{i-1}, v_i)\,. \tag{A.17}$$

If $\mathcal{P}(u,v)$ denotes all possible paths between the two vertices $u$ and $v$, then the *shortest path* $P(u,v)$ between $u$ and $v$ is given as

$$P(u,v) = \arg \min_{P \in \mathcal{P}(u,v)} c(P) \tag{A.18}$$

The value $c(P(u,v))$ is often called the *length* or *distance* between $u$ and $v$.

# B Mathematical proofs

## B.1 Proof of Theorem 3.1

Recall that both intensities $\lambda_H$ and $\lambda_L$ of $X_H$ and $X_L$, respectively, can be expressed by $\lambda_1$, $\lambda_2$, and $\gamma$; see Section 2. In fact, we have

$$\lambda_H = \lambda_1\gamma \qquad \text{and} \qquad \lambda_L = \lambda_2\gamma\,. \tag{B.19}$$

Furthermore, consider the function $f : \mathbb{R}^2 \times [0,\infty) \times \Omega \to [0,\infty)$ given by

$$f(x,c,\omega) = \begin{cases} c & \text{if } X_H(\theta_{-x}\omega, B^{\neq}_{||x||}(x)) = 0\,, \\ 0 & \text{otherwise} \end{cases} \tag{B.20}$$

for any $x \in \mathbb{R}^2$, $c = c(P(x,o)) \geq 0$, and $\omega \in \Omega$. Then, $f(x,c,\omega) = c$ if $-x \in \mathbb{R}^2$ is an atom of the counting measure $X_H(\omega,.)$ such that there are no other atoms of $X_H(\omega,.)$ which are closer (in the Euclidean sense) to the origin $o$ than $-x$. Thus, applying Neveu's exchange formula (A.11), we have that

$$\begin{aligned} \mathbb{E}_{X_L} c(P(o,N(o))) &= \int_{\Omega \times D} \int_{\mathbb{R}^2} f(-x,g,\omega) X_H(\omega,dx) \mathbb{P}^*_{X_L}(d(\omega,g)) \\ &= \frac{\lambda_H}{\lambda_L} \int_{\Omega} \int_{\mathbb{R}^2 \times D} f(x,g,\theta_x\omega) X_L(\omega,d(x,g)) \mathbb{P}^*_{X_H}(d\omega)\,. \end{aligned} \tag{B.21}$$

Notice that given the typical Voronoi cell $\Xi^*$ and the (typical) line system $L(\Xi^*)$ within $\Xi^*$, the (random) number of points of $X_L$ on $L(\Xi^*)$ is Poisson distributed with expectation $\eta = \lambda_2 \nu_1(L(\Xi^*))$. Thus, taking into account the definition of the function $f$ given in (B.20), we get that the inner integral on the right hand side of (B.21) can be expressed in the form

$$\int_{\mathbb{R}^2 \times D} f(x,g,\theta_x\omega) X_L(\omega,d(x,g)) = \sum_{k=1}^{\infty} e^{-\eta} \frac{\eta^k}{k!} \int_{L(\Xi^*)} \dots \int_{L(\Xi^*)} \sum_{i=1}^{k} \frac{c(P(u_i,o))}{\nu_1(L(\Xi^*))^k}\, du_1 \dots\, du_k\,,$$

due to the (conditional) uniform distribution of the lower–level components on $L(\Xi^*)$. Hence,

$$\begin{aligned} \int_{\mathbb{R}^2 \times D} f(x,g,\theta_x\omega) X_L(\omega,d(x,g)) &= \sum_{k=1}^{\infty} e^{-\eta} \frac{\eta^k}{k!} \frac{k}{\nu_1(L(\Xi^*))} \int_{L(\Xi^*)} c(P(u,o))\, du \\ &= \lambda_2 \int_{L(\Xi^*)} c(P(u,o))\, du\,. \end{aligned}$$

Putting things together, we get that

$$\mathbb{E}_{X_L} c(P(o,N(o))) = \frac{\lambda_H}{\lambda_L}\, \lambda_2\, \mathbb{E}_{X_H} \int_{L(\Xi^*)} c(P(u,o))\, du\,.$$

Combining this with (2.2) and (B.19), the theorem is proven. □

## B.2 Proof of Theorem 3.2

We first show that (3.8) holds. If $c(P(B,o)) = c(P(A,o))$, then obviously $c(P(A,B)) \geq |\delta_S| = 0$. Let now $c(P(B,o)) > c(P(A,o))$ and suppose that

$$c(P(B,o)) > c(P(A,B)) + c(P(A,o))\,.$$

Then the path length $c(P(A,B)) + c(P(A,o))$ from $B$ to $o$ via $A$ would be smaller than $c(P(B,o))$, which is a contradiction to the definition of the shortest path length $c(P(B,o))$. Thus, (3.8) is shown. If $c(P(A,B)) = 0$, then, by the monotonicity of $c : E \to [0,\infty)$, we have that

$$c(P(B,u)) = c(P(A,u))$$

for each $u \in S$. Furthermore, (3.8) implies that

$$c(P(B,o)) = c(P(A,o))\,,$$

and i.e., (3.9) and (3.10) are obviously true for any $D \in S$. We now assume that $c(P(A,B)) > 0$. Suppose first that

$$c(P(B,o)) = c(P(A,B)) + c(P(A,o))\,.$$

Then it is easy to see that (3.9) and (3.10) hold for $D = B$. If $c(P(B,o)) > c(P(A,o))$ and

$$c(P(B,o)) < c(P(A,B)) + c(P(A,o))\,,$$

then, by the monotonicity of $c : E \to [0,\infty)$, there is a "distance peak" $D$ which lies between the two endpoints $A$ and $B$, respectively, of $S$; see Figure 6(b). Notice that the distance peak $D$ is characterized to be an inner point of the segment $S$, where $c(P(D,o))$ takes the same value no matter if the origin $o$ is reached via $A$ or $B$. In other words, (3.9) and (3.10) hold. □

## B.3 Proof of Corollary 3.3

Using the abbreviations $c_A(S) = c(P(A,o))$ and $c_B(S) = c(P(B,o))$ as well as $\delta_S = c_B(S) - c_A(S)$ (as already defined in Theorem 3.2) and having in mind that $c(S) = \nu_1(S)$, (3.9) gives that

$$\nu_1(D-A) = \frac{\nu_1(S) + c_B(S) - c_A(S)}{2}\,, \qquad \nu_1(D-B) = \frac{\nu_1(S) + c_A(S) - c_B(S)}{2}\,.$$

Furthermore, we may write (3.10) in the form

$$\int_S c(P(u,o))\,du = f_1(\nu_1(S); c_A(S), c_B(S)) + f_2(\nu_1(S); c_A(S), c_B(S))\,,$$

where

$$f_1(x;\theta_1,\theta_2) = \frac{x+\theta_2-\theta_1}{2}\,\frac{2\theta_1 + 1/2(x+\theta_2-\theta_1))}{2} \tag{B.22}$$

and

$$f_2(x;\theta_1,\theta_2) = \frac{x+\theta_1-\theta_2}{2}\,\frac{\theta_1+\theta_2 + 1/2(x+\theta_2-\theta_1))}{2}\,. \tag{B.23}$$

Notice that $f_1(\nu_1(S); c_A(S), c_B(S))$ is the sum of the first two summands in (3.10), whereas the term $f_2(\nu_1(S); c_A(S), c_B(S))$ is the sum of the last two summands in (3.10). By elementary calculations, we now get that the sum of the expressions in (B.22) and (B.23) gives (3.12). □

## B.4 Proof of Theorem 4.1

Using Neveu's exchange formula (A.11) and proceeding similarly as the proof of Theorem 3.1, we get that

$$\mathbb{E}_{X_L'} c(P(o,N(o))) = \frac{\lambda_H}{\lambda_L}\,\lambda_L\,\mathbb{E}_{X_H}\int_{\Xi^*} c(P(u,o))\,du = \lambda_H\,\mathbb{E}_{X_H}\int_{\Xi^*} c(P(u,o))\,du\,,$$

where in the first equality we used that, given the typical Voronoi cell $\Xi^*$ and the (typical) line system $L(\Xi^*)$ restricted to $\Xi^*$, the random number of points of $X_L'$ within $\Xi^*$ is Poisson distributed with expectation $\eta' = \lambda_L \nu_2(\Xi^*)$. We can then finish the proof by using the fact that $\lambda_H^{-1} = \mathbb{E}_{X_H}\nu_2(\Xi^*)$. □

## B.5 Proof of Theorem 5.1

We only show that (5.1) holds, because the proof of (5.2) is analogous. Let $\gamma^{(2)} = a\,\gamma^{(1)}$ and $\lambda_1^{(2)} = a\,\lambda_1^{(1)}$ for some $a > 0$. Then, we can use the scaling properties of the typical cell $\Xi^{*(i)}$ of the Voronoi tessellation induced by the (Coxian) point process $X_H^{(i)}$ of higher–level components with parameter pair $(\gamma^{(i)}, \lambda_1^{(i)})$; see Figure 9. This gives that

$$\mathbb{E}_{X_H^{(1)}}\int_{L^{(1)}(\Xi^{*(1)})} \nu_1(P^{(1)}(u,o))\,du = a^2\,\mathbb{E}_{X_H^{(2)}}\int_{L^{(2)}(\Xi^{*(2)})} \nu_1(P^{(2)}(u,o))\,du\,, \tag{B.24}$$

where $L^{(i)}(\Xi^{*(i)})$ is the (Palm) line system within $\Xi^{*(i)}$ and $\nu_1(P^{(i)}(u,o))$ is the length of the corresponding shortest path from $u$ to $o$. Thus, by (2.2) and (3.4), we have that

$$\begin{aligned}
\gamma^{(1)}\,c_{LH}^*(\gamma^{(1)},\lambda_1^{(1)}) &= \gamma^{(1)}\lambda_1^{(1)}\mathbb{E}_{X_H^{(1)}}\int_{L^{(1)}(\Xi^{*(1)})} c(P^{(1)}(u,o))\,du \\
&= \frac{\gamma^{(2)}\lambda_1^{(2)}}{a^2}\,\mathbb{E}_{X_H^{(1)}}\int_{L^{(1)}(\Xi^{*(1)})} c(P^{(1)}(u,o))\,du \\
&= \gamma^{(2)}\lambda_1^{(2)}\,\mathbb{E}_{X_H^{(2)}}\int_{L^{(2)}(\Xi^{*(2)})} c(P^{(2)}(u,o))\,du \\
&= \gamma^{(2)}\,c_{LH}^*(\gamma^{(2)},\lambda_1^{(2)})\,,
\end{aligned}$$

where, in the third equality, we used (B.24) together with the assumption that the cost value of any segment of the path $P^{(i)}(u,o)$ is its length. □